

Performance of alumina supported Ni catalyst with core-shell and supported structures in dry reforming of methane

A Thesis Submitted to the College of
Graduate and Postdoctoral Studies in
Partial Fulfilment of the Requirements for the
Degree of Master of Science in the
Department of Chemical and Biological Engineering
University of Saskatchewan
Saskatoon, Saskatchewan

By

Zahra Alipour

© Copyright Zahra Alipour, December 2022. All rights reserved.

Unless otherwise noted, copyright of the material in this thesis belongs to Zahra Alipour

Permission to Use

In presenting this thesis in partial fulfillment of the requirements for a Postgraduate degree from the University of Saskatchewan, I agree that the Libraries of this University may make it freely available for inspection. I further agree that permission for copying of this thesis/dissertation in any manner, in whole or in part, for scholarly purposes may be granted by Professor Ajay. K. Dalai who supervised my thesis work. It is understood that any copying or publication or use of this thesis or parts for financial gain shall not be allowed without my written permission. It is also understood that due recognition shall be given to me and to the University of Saskatchewan in any scholarly use which may be made of any material in my thesis.

Requests for permission to copy or to make other use of material in this thesis in whole or parts shall be addressed to:

Head

Department of Chemical and Biological
3B48 Engineering Building,
57 Campus Drive, Saskatoon, Saskatchewan
S7N 5A9, Canada

or

Dean

College of Graduate and Postdoctoral Studies
University of Saskatchewan
Room 116 Thorvaldson Building, 110 Science
Place, Saskatoon, Saskatchewan
S7N 5C9, Canada

Abstract

Dry reforming of methane is one of the interesting processes in which CH_4 and CO_2 are consumed at the same time and valuable syngas is produced. In this research, $\text{Ni}@\text{Al}_2\text{O}_3$ core-shell structure catalyst is compared with the $\text{Ni}/\text{Al}_2\text{O}_3$ supported catalysts in terms of their catalytic stability, activity and carbon formation in dry reforming of methane. The core-shell structure catalysts were prepared by microemulsion method and impregnation technique was used for the supported catalysts. The Ni loadings were 5- 20 wt. % for the both types of catalysts. The prepared catalysts were analyzed with BET, XRD, TPR, XPS, TEM, XAS, and ICP analysis. BET analyses, TEM, and SEM-EDS images showed that core-shell structure catalysts were successfully prepared with smaller particle size and higher surface area ($\geq 200 \text{ m}^2/\text{g}$) than the supported catalysts ($< 200 \text{ m}^2/\text{g}$). Furthermore, TPR and XPS analysis revealed that NiAl_2O_4 species was the main Ni phase in all the catalysts, making strong interaction between Ni and Al_2O_3 . XANES analysis revealed that all the catalysts were almost reduced completely. The catalytic test reaction was carried out at $750 \text{ }^\circ\text{C}$, $\text{GHSV} = 144 \text{ L. g}^{-1} \cdot \text{h}^{-1}$ and $\text{CH}_4:\text{CO}_2:\text{N}_2 = 1:1:1$. The results demonstrated that core-shell catalysts had better catalytic activity than the supported catalysts due to encapsulation of Ni with shell, preventing Ni particle from agglomeration and sintering in comparison with the supported catalysts. The highest CH_4 and CO_2 conversions belonged to 20% $\text{Ni}@\text{Al}_2\text{O}_3$ catalyst with around 55% and 57%, respectively. Further, H_2/CO ratio was almost 1 for the core-shell catalyst whereas this amount was around 0.9 for the supported catalysts. The lower amount of carbon was also deposited in the core-shell catalysts due to smaller particle size and Ni covered with the shell. The lowest amount ($\sim 2\text{wt.}\%$) of coke deposited on the 12% $\text{Ni}@\text{Al}_2\text{O}_3$ catalysts while this amount was about 5 wt. % for the supported catalysts with the same loading. The long term thermal stability test (24 h) showed great stability for the core-shell structure catalyst while it was gradually deactivated after 120 h in reaction due to carbon formation.

Acknowledgments

I would like to express my deepest appreciation and acknowledgment to my supervisors, Professor Ajay Dalai and Professor Hui Wang, for their distinguished knowledge in catalysis and reaction engineering and their significant support during my master program at the University of Saskatchewan. Their skills in catalysis are greatly appreciated and valued.

My sincere thanks go to Dr. Mohsen Shakouri (Canadian Light Source) for his assistance and informative advice during my research program as well as running XAS analysis for my research.

I would also like to thank my advisory committee members: Dr. Lifeng Zhang (Department of Chemical and Biological engineering) and Dr. Shafiq Alam (Department of Chemical and Biological engineering) for their valuable and informative comments for my research.

My deepest thank go to the Dr. Dalai's research group members, including Dr. Venu Borugadda, Dr. Sonil Nanda, Dr. Philip. E. Boahene, and Dr. Sundar Vedachalam for their assistants during my research period.

I am also grateful to Ms. Rosa Do Phuong, RLee Prokopishyn, and Mrs. Jayasinghe Dushmanthi for their technical supports in the lab.

I am also thankful to Saskatchewan Structure Science Center (SSSC) staffs for their helpings in XRD and XPS analyses.

I would also express my thanks and appreciation to my parent (Farrokh and Emamgholi) and my sisters (Marzieh, Azam, Farzaneh) for all of their kindness and encouragement during my life.

Dedication

To my supportive parent, Farrokh and Emamgholi, for being a great source of love, encouragement, inspiration and patience, I am sure that without your help and support I would not be able to be where I am now.

To my lovely sisters, Marzieh, Azam, and Farzaneh, who are not only the best sisters in the world, but they are also the best friends for me whom I can trust anytime.

Table of Content

Chapter 1. Introduction and Thesis Outline	1
1.1. Introduction	1
1.2. Syngas production through reforming processes	2
1.3. Knowledge gaps	4
1.4. Hypotheses	5
1.5. Objectives.....	5
1.6. Organization of thesis.....	5
Chapter 2. Literature Review	6
2.1. Catalysts deactivation in dry reforming of methane	6
2.2. Heterogeneous catalysts for dry reforming	6
Chapter 3. Research Methodology.....	18
3.1. Catalyst preparation methods	18
3.2. Characterization techniques	19
3.3. Experimental set-up for DRM reaction.....	21
Chapter 4. Results and Discussion.....	24
4.1. Structural properties of the catalysts	24
4.2. TPR analysis of the fresh catalysts.....	27
4.3. Morphology of the fresh catalysts with TEM and SEM analysis	28
4.4. XPS analysis.....	34
4.5. Study of reducibility of the catalysts.....	35
4. 6. Catalytic performance study.....	42
4. 7. Carbon formation	45
Chapter 5. Conclusion and Recommendations	48
5.2. Conclusions	48
5.3. Recommendations	49

References.....	50
Appendix A. Permission to use.....	60
Appendix B. MFC calibration.....	69
Appendix C. GC calibration	71
Appendix D. Temperature profile of the reactor	73
Appendix E. Reproducibility of experimental results.....	74

List of Table

Table 1.1. Biogas sources, CH ₄ and CO ₂ contents and CH ₄ /CO ₂ ratio	2
Table 1.2. Syngas production through various reforming technologies	3
Table 2.1. Noble metal catalysts for DRM.	8
Table 2.2. Non-noble metal catalysts for the dry reforming reaction	9
Table 2.3. Bimetallic catalysts for the dry reforming reaction	11
Table 2.4. Catalysts with different support for the dry reforming reaction	12
Table 2.5. Promoters used for dry reforming reaction.....	14
Table 4.1. Textural and structural properties of the catalysts.....	26
Table 4.2. Bulk and surface amount of Ni	34
Table 4.3. Metal and metal oxide extent in reduced catalysts calculated by linear combination fitting of XANES. Reduction conditions were T= 750 °C for 3 h in H ₂ /N ₂ : 40/60	37
Table 4.4. Comparing different GHSV effect on the activity of the catalyst in DRM	45
Table 4.5. The amount of carbon deposited from CHSN analysis	45
Table E.1. Reproducibility results for Metal dispersion.....	74
Table E.2. Reproducibility results for CH ₄ and CO ₂ conversions in 12%Ni@Al ₂ O ₃ catalyst...74	74

List of Figure




Figure 1.1. Syngas application based on the H ₂ /CO ratio.....	1
Figure 2.1. Model of carbon removal over catalysts with various particle size for DRB. (A) Catalyst with large metal particle sizes. (B) Catalyst with medium metal particle sizes. (C) Catalyst with small metal particle sizes. () Carbon species derived from the dissociative adsorption of CH ₄ on the surface of metal ensemble (M); () Activated CO ₂ on the surface of support (S); ()	7
Figure 2.2. TPO profiles of (1) 5%Ni/Al ₂ O ₃ , (2) 5%Ni/3%Mg–Al ₂ O ₃ , (3) 5%Ni/3%Ca–Al ₂ O ₃ and (4) 5%Ni/3%Ba–Al ₂ O ₃ catalysts.....	13
Figure 3.1. Schematic of catalysts preparation method with supported structure	18
Figure 3.2. Catalyst preparation method with microemulsion method.....	19
Figure 3.3. Set-up used for study of activity test	22
Figure 4.1. (a) N ₂ adsorption/ desorption isotherm (b) Pore size distribution of Ni catalyst with supported and core- shell structure.	25
Figure 4.2. XRD patterns of calcined catalysts with the supported and core- shell structures	27
Figure 4.3. TPR spectra of the catalysts with the supported and core- shell structures.....	28
Figure 4.4. TEM analysis of the fresh supported and core-shell structure catalyst	30
Figure 4.5. Particle size distribution of the fresh catalysts with the supported and core-shell structures	31
Figure 4.6. TEM images of Ni alumina with the core shell and supported structures in other literature (a) Ni@Al ₂ O ₃ (b) Ni/Al ₂ O ₃ (c) Ni@Al ₂ O ₃ with high resolution (d) Ni@Al ₂ O ₃ in this research	32
Figure 4.7. SEM-EDS images of calcined (a) 12%Ni/Al ₂ O ₃ and (b) 12%Ni@Al ₂ O ₃ catalysts	33
Figure 4.8. XPS spectra of supported Ni/Al ₂ O ₃ and core- shell Ni@Al ₂ O ₃	35

Figure 4.9. XRD patterns of reduced catalysts with 12% Ni loading with the supported and core-shell structures.....	36
Figure 4.10. Ni XANES analysis of (a) supported and (b) core-shell structure catalysts reduced at 750 °C for 3 h in the presence of N ₂ :H ₂ = 60:40.....	38
Figure 4.11. TEM analysis of of the reduced catalysts with the supported and core-shell structures	40
Figure 4.12. Particle size distribution of the reduced catalysts with the supported and core-shell structures	41
Figure 4.13. Catalytic reaction test over the supported and core-shell structures catalysts at 750 °C, CH ₄ :CO ₂ :N ₂ =1:1:1, GHSV= 144 (L.g ⁻¹ .h ⁻¹), 5 h conditions. (a) CH ₄ conversion, (b) CO ₂ conversion, (c) rate (CH ₄), (d) rate (CO ₂), (e) H ₂ /CO ratio....	44
Figure 4.14. XRD analysis of the used catalysts after 5 h time on stream	46
Figure 4.15. Long term catalytic stability test for 12% Ni@Al ₂ O ₃ catalyst under 750 °C, (a) 24 h and (b) 120 h time on stream. CH ₄ :CO ₂ :N ₂ =1:1:1, GHSV= 144 (L.g ⁻¹ .h ⁻¹), conditions (●) CH ₄ conversion (▲) H ₂ /CO.....	47
Figure B.1. Flow controller device.....	69
Figure B.2. MFC calibration curves.....	70
Figure C.1. GC calibration curves.....	72
Figure D.1. (a) Furnace temperature calibration curve (b) temperature profile of the reactor.....	73

Nomenclature

ALD	Atomic layer deposition
ATR	Auto-thermal reforming
BJH	Barrett-Joyner-Halenda
BE	Binding energy
BET	Brunauer–Emmett–Teller
CHNS analysis	Carbon, Hydrogen, Nitrogen, Sulfur analysis
DRB	Dry reforming of biogas
DRM	Dry reforming of methane
FWHM	Full width at half maximum
GC	Gas chromatograph
GHGs	Greenhouse gases
GHSV	Gas hourly space velocity
ICP	Inductively coupled plasma
ME	Microemulsion
MFC	Mass flow controller
Ni/Al ₂ O ₃	Alumina supported Ni catalysts (supported structure)
Ni@Al ₂ O ₃	Ni covered by alumina (core-shell structure)
POM	Partial oxidation of methane
SD	Standard deviation
SEM-EDS	Scanning electron microscopy- energy dispersive spectroscopy
SMA	Spherical mirror analyzer
SXRMB	Soft X-ray microcharacterization beamline
SRM	Steam reforming of methane
TEM	Transmission electron microscopy

TPR	Temperature- programmed reduction
XAS	X-ray absorption spectroscopy
XRD	X-ray diffraction
XPS	X-ray photoelectron spectroscopy
XANES	X-ray absorption near edge spectroscopy

Chapter 1. Introduction and Thesis Outline

1.1. Introduction

One of the main problems in 21st century is global warming due to rapid emission of greenhouse gases (GHGs) such as CH₄ and CO₂. The release of GHGs causes ozone layer depletion, glacier melting, and sea level rise, creating many problems for human and animals. 195 countries have adopted “Paris Agreement” to reduce GHGs emission and save our environment. In this regard, many efforts have been made to develop technologies to convert CH₄ and CO₂ gases via dry and steam reforming of methane to valuable products. In dry reforming, CH₄ and CO₂ are converted to valuable syngas. The produced syngas is utilized as a feedstock in production of other materials based on H₂/CO ratio, as can be seen in Figure 1.1 (Gao et al., 2018).

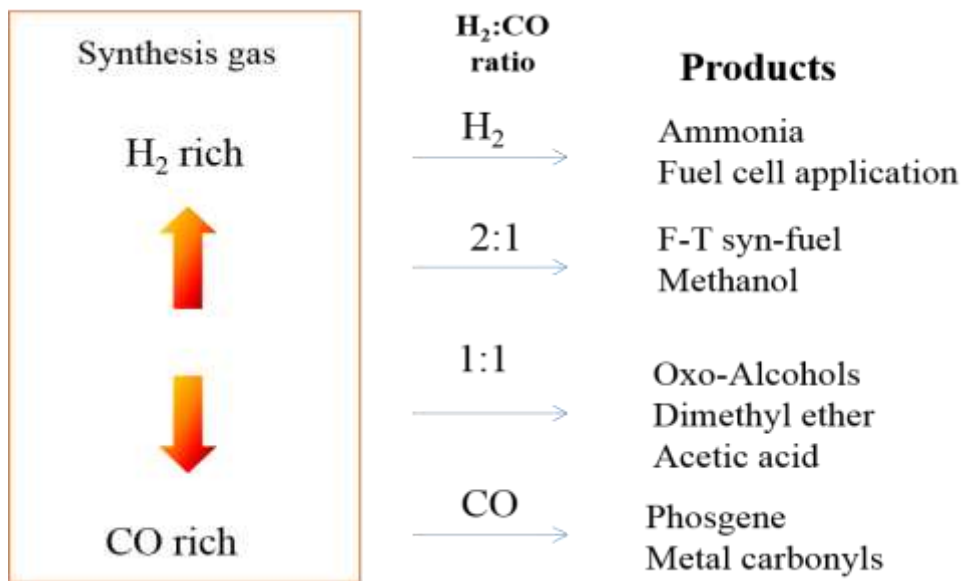


Figure 1.1. Syngas application based on the H₂/CO ratio

Furthermore, biomass conversion to bio-oil and renewable energies has been increasing due to global warming as well as fossil fuel depletion. In this regard, biogas, derived from anaerobic digestion process, has attracted tremendous attention as a renewable, and environmentally sustainable source for gaseous biofuel for the generation of heat and power (Rosset et al., 2020). What's more, two main components of this gas, CH₄, and CO₂, can be utilized instead of releasing

them to the environment, which benefits climate change. Dry reforming of biogas has been widely considered to achieve this. In this process, CH₄ and CO₂ react in the presence of a suitable catalyst at suitable process conditions, and syngas (a mixture of H₂ and CO) is produced (Eq. (1-1)). It is worth noting that the dry reforming of biogas (DRB) is the same as dry reforming of methane (DRM) reaction (called model biogas) with a higher amount of CH₄. CH₄/CO₂ molar ratio in biogas depends on the biogas sources (Table 1.1) (Gao et al., 2018; Zhan et al., 2017)

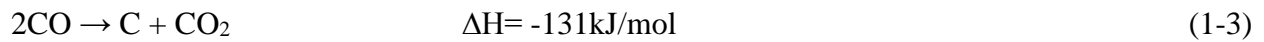
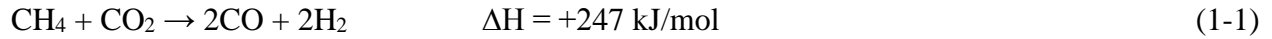


Table 1.1. Biogas sources, CH₄ and CO₂ contents and CH₄/CO₂ ratio (Gao et al., 2018)

Biogas Source	CH ₄ content (%)	CO ₂ content (%)	CH ₄ /CO ₂ molar ratio
Model biogas	50	50	1
Landfill Waste	55	45	1.25
Sewage Waste	60	40	1.5
Organic Waste	65	35	1.85

The produced syngas can be used in reactions such as Fischer- Tropsch, and methanol production. Additionally, produced hydrogen can be employed in fuel cells to generate electricity (Das et al., 2022) .

1.2. Syngas production through reforming processes

As it is mentioned earlier, syngas is produced through reforming technologies such as steam reforming of methane (SRM), dry reforming of methane (DRM), partial oxidation of methane (PON), and auto-thermal reforming of methane (ATR). These processes are shown in Table 1.2 (Li et al., 2008; Abatzoglou et al., 2016)

Table 1.2. Syngas production through various reforming technologies

Reactions			H ₂ /CO ratio
Dry reforming of methane (DRM)	CH ₄ + CO ₂ → 2H ₂ + 2CO	ΔH = +247 kJ/mol	1
Reverse Water Gas Shift	CO ₂ + H ₂ → CO + H ₂ O	ΔH = +41.8 kJ/mol	
Steam reforming of methane (SRM)	CH ₄ + H ₂ O → 3H ₂ + CO	ΔH = +205.8 kJ/mol	3
Water Gas Shift	CO + H ₂ O → CO ₂ + H ₂	ΔH = -41.8 kJ/mol	
Partial oxidation of methane (POM)	CH ₄ + 0.5O ₂ → 2H ₂ + CO	ΔH = -36 kJ/mol	2
Auto-thermal reforming of methane	CH ₄ + 0.5O ₂ → 2H ₂ + CO		2-3
	CH ₄ + H ₂ O → 3H ₂ + CO		

In SRM reaction, CH₄ reacts with H₂O and syngas with H₂/CO ratio of 3 is produced. This reaction is highly endothermic and requires high energy to operate. One of the main issues in this reaction is consumption of H₂O as well as production of CO₂ through water gas shift reaction. Partial oxidation of methane has been used for production of syngas but it requires oxygen. Auto-thermal reforming reaction, which is combination of steam reforming and partial oxidation methane, is another process used for syngas production. This reaction needs H₂O and O₂ at the same time, which makes this process less affordable. Dry reforming of methane has attracted much interests as two main greenhouse gases (CH₄ and CO₂) are consumed at the same time and valuable syngas is produced (Carapellucci et al., 2020).

The main challenge of the DRM is a rapid coke formation, rooting from CH₄ decomposition (Eq. (1-2)) and Boudouard reaction (Eq. (1-3)), resulting in the catalyst deactivation and reactor blockage. Filamentous type carbon or carbon nanotubes is highly produced in dry reforming, pushing the active metal particle and causing it to disconnect from the support (Alipour et al., 2023; Shamskar et al., 2017). It is also reported that sulfur in biogas causes catalyst poisoning and deactivation, which is another issue in this process. Furthermore, sintering of active metals is another problem for the catalysts used in this process, which is coalescence of active metals due to high temperature (Alipour et al., 2014c). Since carbon formation highly depends on the composition and structure of the catalyst, many efforts have been made to solve these problems. It is worth noting that catalyst sintering, strong metal-support interaction, and the basicity of support, could remarkably decrease the catalyst deactivation. Various catalysts have been proposed by researchers for this process to suppress the deposited coke and boost the catalytic activity (Aziz et al., 2019). It is reported that noble metals based catalysts (Rh, Ru, Pt, Pd) have a great catalytic

performance with the lower carbon deposition but they are rarely used due to their high price and scarcity (Nematollahi et al., 2011). Non-noble metals catalysts like Ni and Co are vastly employed for this process because of their abundance and lower cost, however severe coke formation is the main issue (Chein et al., 2019). It is worth noting that different supports, promoters, preparation methods, and reaction conditions could remarkably lower the deposited carbon and improve the catalytic activity and stability in dry reforming. Among the supports, Al₂O₃ is highly recommended owing to its higher surface area, culminating in better Ni dispersion and smaller particle size. CeO₂, ZrO₂, SiO₂, and MgO are other supports widely used in dry reforming (Zhang et al., 2015). Another way to reduce coke deposition in dry reforming catalysis is the addition of promoters such as CeO₂ or alkaline earth promoters (MgO, CaO, BaO, SrO), causing catalytic performance improvement due to oxygen storage capacity of CeO₂ and basic properties of alkaline earth promoters, resulting in CO₂ adsorption enhancement and hindering Boudourd reaction and coke suppression (Alipour et al., 2014b). Moreover, as bimetallic samples could provide more active sites for reactants and as a result higher conversions could be achieved, Co, Cu, Fe, and Mo are incorporated with Ni as a second metal in dry reforming (Bian et al., 2017a). Core/yolk@ shell type catalyst is another configuration, which significantly shows the great catalytic behavior and lower carbon deposition in dry reforming due to encapsulated active metals in the shell, inhibiting the active metal sintering and prolonging the catalyst lifetime (Li et al., 2019). Further, catalysts preparation methods, calcination, and reduction temperatures significantly play essential roles in the catalytic performance. In the regard to catalytic preparation methods, impregnation, co-precipitation, sol-gel routes are widely used, while sol-gel has been suggested as the better preparation method, which can produce catalysts with higher metal dispersion with the stronger metal-support interaction (Usman et al., 2015).

1.3. Knowledge gaps

Based on the literature review discussion in Chapter 2, the identified knowledge gaps are as follows:

1. Study of core@shell catalyst in dry reforming of methane as compared to supported catalyst at high GHSV is missing in the literature.
2. Comparing the core-shell and supported catalysts in terms of particle size and reducibility after reduction

1.4. Hypotheses

The following hypotheses are made:

1. It is hypothesized that core@shell catalysts show better catalytic performance compared to supported ones in dry reforming of methane due to alleviation of the amount of deposited coke and sintering, as a result of smaller particle size, and encapsulation and protection of nanoparticles by an outer shell.
2. It is assumed that core-shell catalyst has better reducibility than the supported ones.

1.5. Objectives

Overall objective: Conversion of methane to syngas through dry reforming reaction.

Sub-objectives:

1. Synthesis of Ni@Al₂O₃ with microemulsion (ME) method and Ni/Al₂O₃ with impregnation method, as a reference catalyst.
2. The prepared catalysts were used in DRM reaction and the supported and core-shell structures catalysts are compared.

1.6. Organization of thesis

This master thesis organized in five chapters. It is structured according to the manuscript-style thesis guidelines of the College of Graduate and Postdoctoral studies. Chapter 2 has been published as a book chapter. The manuscripts described in Chapters 4 has been submitted to Chemical Engineering Journal.

An introduction to the subject matter is given in Chapter 1. Chapter 2 presents relevant literature reviews of dry reforming of methane, catalysts used in this reaction, and rout to improve catalytic activity. In Chapter 3 the experimental procedures are discussed, including all the materials, processes (DRM) and techniques used to prepare and characterize catalysts used in this study. In Chapter 4, the prepared catalysts were characterized with different techniques such as XRD, TPR, BET, XPS and etc, and used in dry reforming of methane reaction to evaluate their performance in terms of activity and stability. The results of catalytic activity and used catalyst's characterizations are also provided in this chapter.

Chapter 5 provides the overall conclusions and recommendations from this research study. The references for all the chapters are collected in the References section, and appropriate additional information is provided in the Appendices.

Chapter 2. Literature Review

The content of this chapter has been published as a book chapter cited below:

Zahra Alipour, Venu Babu Borugadda, Hui Wang, Ajay K. Dalai, Chapter 8- Dry reforming of methane and biogas to produce syngas: a review of catalysts and process conditions, Editors: Sonil Nanda, Dai-Viet N. Vo, and Van-Huy Nguyen, 2022, Elsevier: Carbon dioxide Capture and Conversion, 201-235.

This chapter includes a literature review on what have been studied on the catalytic activity and stability of the catalysts used in DRM.

2.1. Catalysts deactivation in dry reforming of methane

As it is noted earlier, one of the main problems in DRM is coke formation through Eq. (1-2) and Eq. (1-3). The formed coke covers active sites and prevents accessibility of reactants to active sites. Moreover, filamentous form of carbon causes active metal detachment from the support and deactivates the catalysts when used for long period of time. Since this reaction (1-2) is an endothermic and operate at higher temperature, sintering and metal coalesce are other issues in this process. It is known that biogas contains impurities such as sulfur, causing catalyst poisoning and deactivation due to adsorption of sulfur with active metals ($M + H_2S \leftrightarrow M-S + H_2$ (M refers to metal)) (Jablonski et al., 2015). Many studies have been carried out to overcome these problems, which are discussed below.

2.2. Heterogeneous catalysts for dry reforming

Many catalysts have been proposed for DRM reaction 20 years ago. Most studies in 2000-2010 have been focused on noble metals catalysts (such as Rh and Ru) and non-noble metals catalysts (such as Ni and Co) with various supports such as alumina, silica, and ceria

García-Diéguez et al., (2012) showed that NiPt/Al₂O₃ catalyst showed great catalytic performance in dry reforming of methane. Furthermore, it is reported that Ni/MgO promoted with Pt showed high catalytic performance and low amount of coke deposition in DRM (Yabe et al., 2018). Whereas from 2010 up to now, most studies have been carried out to modify non-noble catalysts with higher activity and lower coke deposition due to noble metals' prices and scarcity.

In this regard, different preparation methods have been studied to decrease metal particle size and increase surface area of the catalysts. Moreover, reaction conditions and use of modifiers are other

variables, which have been widely investigated to increase lifetime of the catalyst. Most of the studies related to dry reforming of methane have focused to design catalysts, which are resistant toward coke formation, sintering, and poisoning. It is also noted that a promoted catalyst should have small particle size, leading to inhibition of coke formation based on the mechanism shown in Figure 2.1. In this figure, it is seen that the catalysts with smaller particle size have lower amount of deposited carbon than those with larger particle size (Zhang et al., 2008). The removal reaction of carbon is due to $S\text{-CO}_2 + M\text{-C} \leftrightarrow 2\text{CO} + S + M$ in which M and S refer to metal active particle and support, respectively.

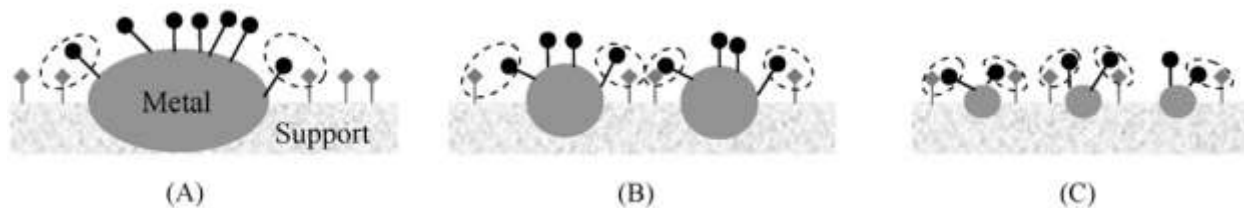


Figure 2.1. Model of carbon removal over catalysts with various particle size for DRB. (A) Catalyst with large metal particle sizes. (B) Catalyst with medium metal particle sizes. (C) Catalyst with small metal particle sizes. (\bullet) Carbon species derived from the dissociative adsorption of CH_4 on the surface of metal ensemble (M); (\uparrow) Activated CO_2 on the surface of support (S); (\circ) (Zhang et al., 2008)

It is noted that larger surface area contributes to better metal dispersion, smaller particle size, avoiding metal coalesce, lower amount of coke deposition, and better catalytic performance

Studies have shown that noble metals based on group VIII, which are known to be active and stable for the reaction, can be incorporated on suitable support. The order of activity has been reported as follows: $\text{Ru} \approx \text{Rh} > \text{Ir} > \text{Pt} > \text{Pd}$. For example, metals such as Rh and Ru have high activity for CO_2 dissociation, with no significant carbon deposition during the reaction (Damyanova et al., 2009; Usman et al., 2015; Fonseca et al., 2020). Nematollahi et al., (2011) confirmed that Rh and Ru supported on MgAl_2O_4 catalysts had higher methane conversion in dry reforming of methane compared to other noble catalysts. Furthermore, all noble metal catalysts represented high stability during 50 h on stream. Similar results have been concluded by Rezaei et al., (2006) for noble

metals supported on alumina magnesia spinel. Noble metal catalysts used in DRM are summarized in Table 2.1.

Table 2.1. Noble metal catalysts for DRM.

Catalyst	Support	Preparation Method	Process Conditions	Reference
Ir – 1 %	γ -Al ₂ O ₃ , 8 mol% Y ₂ O ₃ stabilized ZrO ₂ (YSZ: Zr _{0.92} Y _{0.08} O _{2-δ}), 10 mol% Gd ₂ O ₃ doped CeO ₂ (GDC: Ce _{0.9} Gd _{0.1} O _{2-δ})	Wet impregnation	400–850 °C, 9000, 11,000 and 18,000 L/g/h (GHSV), 12 h,	(Yentekakis et al., 2015)
Pd	CeO ₂	Single-step surfactant induced method	350 °C, 12 h	(Singha et al., 2017)
Pd	Hydroxyapatite	Ultrasound-assisted ion exchange (IE) and incipient wetness impregnation (IWI)	Feed: 100 mL. min ⁻¹ comprising CH ₄ :CO ₂ :He equal to 5:5:90, 0.2 g _{cat} , 200 and 650 °C	(Kamieniak et al., 2017)
Pt, Ru	MgO- Al ₂ O ₃ , ZrO ₂ - Al ₂ O ₃ , CeO ₂ - Al ₂ O ₃ , and La ₂ O ₃ - Al ₂ O ₃	Incipient wetness impregnation (IWI)	650 °C with a 1:1:1 molar ratio of CH ₄ :CO ₂ :N ₂ gas mixture	(Oliveira et al., 2014)
Pt	Al ₂ O ₃		P=1 atm, CH ₄ /CO ₂ /N ₂ =1:1:8, GHSV=120, 240 L/g _{cat} /h; T=700 °C, t=18 h.	(Li et al., 2015)
Pt, Ru	Pyrrhlores	Modified Pechini method	600-min, 50 mg cat, GHSV= 48,000 mL/g _{cat} /h	(Pakhare et al., 2013)
Rh, Ru, Pt, Pd, Ir (1 wt.%)	Alumina	Wet impregnation	GHSV= 16000L/kg _{cat} / h, 150 mg cat, 600 °C for 2 h	(Nematollahi et al., 2011)

Ni-based catalysts are extensively used in dry reforming processes with various supports due to availability and lower cost compared to noble metals (García-Diéguez et al., 2012). For instance, it is reported that Ni/Al₂O₃ showed good catalytic activity but it deactivated due to coke formation. Additionally, Ni/MgAl₂O₄ had better catalytic stability in dry reforming due to spinel MgAl₂O₄, causing strong interaction between Ni and support (Guo et al., 2004). Ni/ZrO₂ showed high catalytic activity reported by Rezaei et al., (2006) for dry reforming as well. Ni/Al₂O₃ prepared by sol-gel methods showed great stability in time on stream of 100 h in dry reforming of methane (Luna et al., 2000). Moreover, other metals like Co has been researched in dry reforming. For instance, Mirzaei et al., (2015) investigated Co/MgO catalysts in dry reforming of methane with various cobalt loadings. The results displayed that the catalyst with 10% Co had the best thermal stability. This can be due to the fact that lower amount of Co content was not catalytically active whilst higher amount of Co caused pore blockage. Table 2.2 summarized the common active metal used in DRM

Table 2.2. Non-noble metal catalysts for the dry reforming reaction

Catalyst	Support	Preparation Method	Reaction Conditions	Reference
Yolk-shell structured Ni	SiO ₂	Reverse micelle approach	1 atm, 700 °C, CH ₄ :CO ₂ = 1:1, GHSV 60 L g ⁻¹ h ⁻¹ , 30 h	(Wang et al., 2019)
Ni	Al ₂ O ₃		P=1 atm, CH ₄ /CO ₂ /N ₂ =1:1:8, GHSV=120, 240 L g _{cat} ⁻¹ h ⁻¹ , T=700 °C, t=18 h.	(Li et al., 2015)
Yolk-shell structured Ni and Ni	SiO ₂	Micro emulsion approach, wetness impregnation	molar ratio CH ₄ /CO ₂ = 1, 100 mg cat, molar ratio CH ₄ /CO ₂ = 1, 600- 750 °C, 1 h	(Wang et al., 2016)
Co (5, 10, 15, 20 and 30 wt.%)	MgO	Co-precipitation	50% CH ₄ and 50% CO ₂ , 200 mg cat, gas hourly space velocity (GHSV) of 12,000 ml/h/g _{cat} , 550 to 700 °C, for 5 h	(Mirzaei et al., 2015)
Ni (core-shell structures)	SiO ₂		40 h, 850 C, 26.8% CO ₂ /26.8 CH ₄ %/46.4% He stream, 20 mg cat	(Zhang & Li, 2015)
Ni	Al ₂ O ₃	Impregnation	CH ₄ :CO ₂ =1:1; total flow 40 mL/min), 550 – 700 °C	(Alipour et al., 2014b)

It has been reported that bimetallic catalysts could remarkably exhibit better catalytic performance compared to monometallic catalysts in dry reforming. The synergetic effect of second metal helps to enhance dispersion as well as provides additional active sites (Jang et al., 2019).

For example, Co, Fe, and Cu exhibited low catalytic activity when employed as a monometallic catalyst, whilst they played a pivotal role as a bimetallic in dry reforming (Gao et al., 2018). The effects of Fe were evaluated for the catalytic performance of Ni/ MgO catalyst in DRM. The coke resistance property of Ni- Fe was ascribed to oxyphilicity of Fe, which resulted in more CO₂ adsorption and more oxygen coverage on the surface, contributing to carbon oxidation. Catalytic deactivation occurred in the presence of excess oxygen, due to the oxidation of metals, whereas Fe/Ni ratio played a considerable role in the catalytic activity and coke formation in this process (Zhang et al., 2020).

The results revealed that Co enhanced catalytic performance and reduced coke deposition. This is likely because of enhancement of CO₂ adsorption by adding Co due to Co-O interactions, culminating in inhibition of coke deposition. In addition, Ni helps to prevent Co from oxidation. Similar results were confirmed by other researchers (Ay et al., 2015; Jawad et al., 2019).

J. Zhang et al., (2007) prepared Ni-Me- Al-Mg-O (Me = Co, Fe, Cu, or Mn) bimetallic catalysts and employed it for dry reforming of methane. The results showed that Ni-Co catalyst had higher catalytic performance and lower amount of coke deposition in dry reforming due to synergetic effect of second metal and just lower amount of Ni-Co content positively affect the catalytic performance due to better dispersion and smaller particle size (Zhang et al., 2008).

Ni-Mn/Al₂O₃ bimetallic catalyst was evaluated in dry reforming of methane to investigate the role of Mn in the catalytic activity of Ni/Al₂O₃ catalyst. The results showed better catalytic activity and less coke formation for the bimetallic sample compared to the monometallic one. This may due to better Ni dispersion and smaller Ni particle size by adding Mn. Furthermore, a moderate amount of Mn had positive effect on the catalytic performance (Ramezani et al., 2018) Macario et al., (2019) found that adding Rh to Ni- based catalysts improved the reducibility of Ni particles. This may due to the interaction between nickel and rhodium oxides that, during the thermal reduction, favors the reduction of nickel oxides by pre-reduced Rh particles. Totally, the addition of noble metals to Ni-based catalysts helps to prevent oxidation of Ni and promote the reducibility of Ni, resulting in more available active sites and catalytic behavior improvement. It is also reported that a low amount of noble metal addition could change the surface properties of Ni (Pakhare et al., 2014; Bian et al., 2017b). Bimetallic catalysts for the dry reforming reaction listed in Table 2.3.

Table 2.3. Bimetallic catalysts for the dry reforming reaction

Catalyst	Support	Preparation Method	Reaction Condition	Reference
NiPt	Al ₂ O ₃	Incipient wetness impregnation	P=1 atm, CH ₄ /CO ₂ /N ₂ =1:1:8, GHSV=120, 240 L/g _{cat} /h, T=700 °C, t=18 h.	(Li et al., 2015)
Ni-based supported monometallic Mo, bimetallic Fe-Mo and Pt-Mo, and trimetallic Pt-Fe-Mo	Al ₂ O ₃ -CeO ₂	Incipient wetness impregnation	300 mg cat, 10 h, temperature 550–700 °C, P =1 bar; feed gas pure CH ₄ and CH ₄ /CO ₂ = 50/50, flow rate =60 mL min ⁻¹ , WHSV = 12,000 mL h ⁻¹	(Jawad et al., 2020)
Bimetallic Ni-Co	MgO	Incipient wetness impregnation	550 to 700 °C, 200 mg cat, 5 and 15 h time-on-stream, CH ₄ :CO ₂ = 1:1, GHSV = 12 000 mL h ⁻¹	(Mirzaei et al., 2014)
10 (wt%) Ni-3 (wt%) Mn	Al ₂ O ₃	Sol-gel method, Wet impregnation	CH ₄ /CO ₂ =1/1,GHSV=12,000 (mL/h.gcat), 200 mg, 700 °C	(Ramezani et al., 2018)
Ni, Ni-Co	CeO ₂	Incipient wetness co-impregnation	600–850 °C, atmospheric pressure and a CH ₄ /CO ₂ ratio of 1, (CH ₄ /CO ₂ /N ₂ = 0.3:0.3:0.4), 0.5 g,	(Turap et al., 2020)
Rh-Pt	Al ₂ O ₃ -La ₂ O ₃	Wet co-impregnation	CH ₄ :CO ₂ :He 10:10:80 vol.% and a total flow rate of 5L/ h, .5 g cat, 300–900 °C,	(Ghelamallah et al., 2014)
Co-Mo–MgO	MWCNTs	Sol–gel technique, CCVD	80 mg, 850 °C, a GHSV of 132L/h/g _{cat} and a CH ₄ /CO ₂ ratio of 1, 650 – 850 °C, 4 h	(Khavarian et al., 2015)

Typically, support itself is not catalytically active, but it participates in the reaction while interacting with the active sites. Aziz et al., (2019) reported that the activity of metal-based catalysts is significantly influenced by the supports, as they impact the dispersion of metal particles, oxygen vacancies, and metal-support interaction. Mesoporous materials as supports are of extensive interest due to high surface area, high pore volume, and uniform pore size, helping active metals have better dispersion (Gao et al., 2018). Ni oxide catalysts have been vastly investigated due to their proper physical and chemical properties. Ni- based oxide catalysts with various supports (SiO₂, Al₂O₃, MgO, ZrO₂, and TiO₂) have been studied for DRM. The findings showed that the catalytic activity followed the order of NiO/Al₂O₃ ≥ Ni/MgO > Ni/SiO₂ > Ni/ZrO₂ > Ni/TiO₂, revealing that the diversity in support material noticeably influenced the activity of the catalyst (Zhang et al., 2015).

Ni- based catalysts with various supports (MgO, ZnO, CeO₂, Al₂O₃, and SiO₂) were prepared and employed for dry reforming of biogas. In this case Ni/Al₂O₃ catalyst showed higher catalytic activity among all due to strong interaction between metals and support, while it caused the reactor blocking owing to carbon deposition in the long run. The catalyst with MgO support had lower

activity compared to Ni/Al₂O₃ but it was more stable. Three other catalysts displayed weak activity in dry reforming of biogas. As a result, Ni/MgO catalyst had the best catalytic performance for this process (Gao et al., 2020) . Common used supports in DRM is shown in Table 2.4.

Table 2.4. Catalysts with different support for the dry reforming reaction

Catalyst	Support	Preparation Method	Reaction Condition	Reference
Ni	Al ₂ O ₃ and MgAl ₂ O ₄	incipient wet impregnation	pressure (1 bar), space-time (2.005 g-h/mol of CH ₄), DRM (CH ₄ :CO ₂ :N ₂ =1:1:1)	(Chaudhary et al., 2020)
Ni	Al ₂ O ₃ , SiO ₂ , MgO, CeO ₂ and ZnO	wet impregnation method	650 - 850°C for 12 h, simulated biogas (CH ₄ /CO ₂ /N ₂ =2:2:1) with an inlet flow rate of 50 mL/min and gas hourly space velocity (GHSV) of 15000 mL/g _{cat} /h	(Gao et al., 2020)
Ni	SiO ₂ , TiO ₂ and ZrO ₂		60000 mL/(gcat·h), 100 h, 750 °C	(Wang et al., 2016)
Rh	CeO ₂	Hard template method	21 h, 650 °C	(Djinović et al., 2012)
Ni	CeO ₂ , ZnO	Impregnation	CH ₄ /CO ₂ =1.5/1, 12 h, 650-900°C	(Rosha et al., 2019)

As mentioned earlier, one of the main drawbacks of Ni catalysts in dry reforming processes is coke formation and catalyst sintering, due to Boudouard reaction ($\text{CO} \leftrightarrow \text{C} + \text{CO}_2$) and methane decomposition. Many studies were carried out to boost catalyst activity and decrease coke formation. One of them is by adding promoters and modifiers to the catalysts. Alipour et al., (2014b) reported that the alkaline earth promoters (MgO, CaO, and BaO) dramatically improved the catalyst activity of Ni/Al₂O₃ for DRM (Figure 2.2). This is likely due to the basicity of the catalysts that enhanced activity, culminated in an increase in CO₂ adsorption and inhibited Boudouard reaction and as a result, the amount of coke formed significantly decreased by adding alkaline earth modifiers.

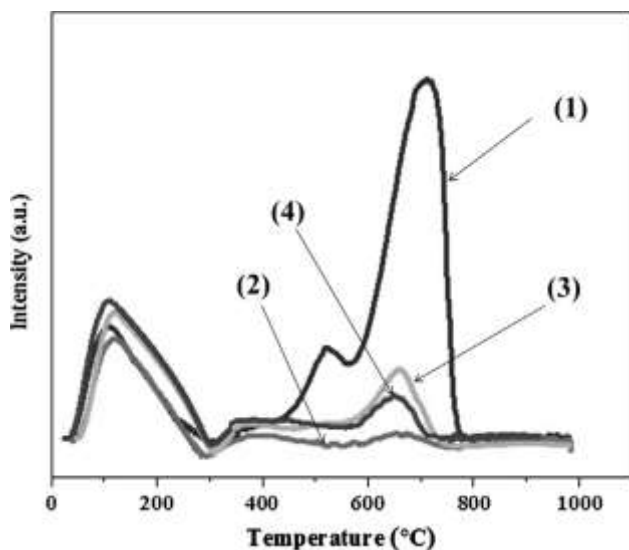


Figure 2.2. TPO profiles of (1) 5%Ni/Al₂O₃, (2) 5%Ni/3%Mg–Al₂O₃, (3) 5%Ni/3%Ca–Al₂O₃ and (4) 5%Ni/3%Ba–Al₂O₃ catalysts (Alipour et al., 2014b)

A similar investigation was carried out by Ghods et al., (2016), validating the positive effects of alkaline earth promoters toward the catalytic activity of the Ni/ MgSiO₃ catalysts. Further, Park et al., (2018) found that an optimum amount of Zn could enhance the catalytic activity and stability of Co/ZrO₂ for DRM. It has been illustrated that promoted supports could dramatically improve the catalyst performance for this reaction. For this purpose, Rezaei et al., (2019) synthesized Ni/ M- MgAl₂O₄ (M= CeO₂, ZrO₂, La₂O₃) and employed them for DRM. The findings displayed that incorporation of the promoters into the catalyst support moved the T_{max} of the reduction peak to a higher temperature, showing the stronger interaction between the metal and support in these samples. Adding CeO₂ as a promoter improved catalytic activity and decreased coke formation compared to other studied promoters for DRM, rooting from redox properties of the catalyst support by adding ceria. The higher amount of modifier caused pore blockage, consequently decreased catalytic activity while smaller amount could not modify properties, reported by (Alipour et al., 2014b). Promoters used for dry reforming reaction is listed on Table 2.5.

Table 2.5. Promoters used for dry reforming reaction

Catalyst	Promoter	Preparation Method	Reaction Conditions	Reference
Ni/ Al ₂ O ₃	MgO	Co-precipitation	550 °C to 700 °C, 200 mg cat, 700 min, CO ₂ /CH ₄ = 1 mol; GHSV= 1.8×10 ⁴ ml/h/g _{cat}	(Mirzaei et al., 2015)
Ni/ Al ₂ O ₃	MgO	Wet impregnation	550 to 700 °C, 200 mg, CH ₄ /CO ₂ = 1/1, GHSV = 12000 mL/(g _{cat} ·h)	(Alipour et al., 2014c)
Ni/ Al ₂ O ₃	MgO, CaO, and BaO	Wet impregnation	CH ₄ /CO ₂ =1/1, GHSV= 12,000(ml/h/g _{cat}), 200 mg, 550 – 700 °C, 1400 min	(Alipour et al., 2014b)
Ni/ Al ₂ O ₃	K ₂ O, MgO, CaO and BaO	Microemulsion	Reaction conditions: CH ₄ /CO ₂ =1, GHSV=18,000 (ml/h·g _{cat}), 250 min,	(Shiraz et al., 2016)
Ni/ Al ₂ O ₃	K ₂ O	Wet impregnation	CH ₄ /CO ₂ =1/1, GHSV= 12,000(ml/h/g _{cat}), 200 mg, 550 – 700 °C, 1400 min	(Alipour et al., 2016)
Rh/ Al ₂ O ₃	La ₂ O ₃	wet impregnation	CH ₄ :CO ₂ :He 10:10:80 vol.% and a total flow rate of 5 L/h, .5 g cat, 300–900 °C,	(Ghelamallah et al., 2014)
Pt/ Al ₂ O ₃	La ₂ O ₃	wet impregnation	CH ₄ :CO ₂ :He 10:10:80 vol.% and a total flow rate of 5 L/h, .5 g cat, 300–900 °C,	(Ghelamallah et al., 2014)
Ni/ MgSiO ₃	CaO, MgO, and BaO	hydrothermal method	CH ₄ /CO ₂ = 1:1, GHSV= 18000 ml/g _{cat} /h, 100 mg, 250 min, 700 °C	(Ghods et al., 2016)

It is also reported that the catalyst preparation method has a significant influence on the interaction between active sites and the support. There are some common preparation routes, used in the catalyst preparation such as the sol-gel, impregnation (incipient and wet), precipitation, co-precipitation, surfactant- assisted, and polyol methods. Since the sol-gel method contributes to strong metal- support interactions and a smaller particle size compared to other methods, it is highly recommended for dry reforming process. It is also explained that precipitated catalysts have lower catalytic activity and stability compared to those produced with the impregnation and sol-gel ones, which is attributed to the lower concentration of active sites and partial oxidation of Ni metal with CO₂ (Arora et al., 2016). Moreover, pore blockage is another issue, seen in the co-precipitated samples whereas NiO particles with the crystal sizes of 9-11 nm could be observed in

the impregnated ones (Arora et al., 2016). It is also reported that the impregnation method has several advantages such as ease of operation and metal distribution control on the support but weak interaction between metal and support (Gao et al., 2018).

The impregnation method is the most common method for preparing metal-supported catalysts. Although it is so difficult to obtain a narrow particle size distribution, it is possible to prepare small metal particles in this method. Furthermore, synthesizing the catalysts with plasma treatment can disperse nickel more than that using the impregnation method (Usman et al., 2015). It is also found that the morphology of the catalyst support has some effect on the structure and size of the metal particles in impregnation method. It is difficult to control the composition of bimetallic particles, whilst it is expected to be a suitable environment for producing small metal nanoparticles with narrow size distributions as well as bimetallic particles production with the controlled composition in the microemulsion route owing to the specific structure of this technique. Besides, it is claimed that microemulsion can provide better interaction between active metal and catalyst support. As a result, this method causes the particle size in the nanometer range, narrow size distribution, and homogeneous composition, making them excellent catalyst precursors (Aboonasr et al., 2016)

One of the major problems in the supported catalysts, especially those based on Ni, is the sintering of active species causing inactive carbon formation. Control the size of a nickel with various catalyst preparation methods is one the solution to overcome this problem (Dekkar et al., 2020). Rezaei et al., (2008) claimed that the synthesis of nanopowder ZrO_2 with the surfactant-assisted method could significantly increase the BET surface area which is one of the main goals in the preparation of the catalysts. Also, Ni impregnated on this support showed high stability after time on the stream of 50 h. Dekkar et al., (2020) studied the influence of microemulsion and impregnation catalysts preparation methods on the catalytic performance of Ni/ Al_2O_3 and Ni/ SiO_2 in DRM. The findings indicated that the catalytic performances are much more dependent on the support properties and that they are deeply influenced by the catalyst synthesis method. The catalytic characterization showed that Ni dispersed on Al_2O_3 and SiO_2 support much higher in the microemulsion method compared to two other catalysts prepared with impregnation. The single phase of NiO was detected for those prepared by impregnation method while it cannot be seen for catalysts prepared by microemulsion, representing high dispersion of NiO.

It is also reported that Cu/SiO₂ coated with ZnO through ALD had smaller Cu particles with better distribution and strong metal-support interaction, which favors the catalytic performance (Gao et al., 2020)

2.3. Dry reforming studies in U of S

It is noteworthy to mention that studies have been done at the U of S from 2008 -2020 for dry reforming of methane. The following studies were carried out by Dr. Dalai and Dr. Wang groups about Ni-based catalyst for dry reforming of methane.

1- Ni-M (M=Co, Cu, Mn, and Fe) - Al-Mg-O catalysts prepared by co-precipitation method and employed in dry reforming reaction. The results showed that Ni-Co bimetallic catalyst had higher surface area, great stability and activity with lower amount of coke deposition compared to other samples. It is also noted that lower amount of Ni-Co content catalytically performed better (Zhang et al., 2007; Zhang et al., 2008).

2- The impact of reduction on the growth of the metallic nanoparticles was studied. The XAS results showed that Co mitigated reduction of Ni while Co reduction were improved by Ni, and there was a strong interaction between Ni and Co atoms leading to the formation of Ni-Co alloy (Wang et al., 2013)

3- Influence of support structure (basic properties of the catalyst) on the catalytic performance of the catalyst was studied. The results illustrated that MgO-solid phase and spinel structure were observed at a higher Mg/Al ratio, and only spinel structure was detected at the lower ratio. The MgO phase boosted the basicity and reduction of the active metals, leading to higher catalytic performance of catalyst for DRM reaction (Alabi, 2018)

4- Ni-Co-Al-Mg-O catalysts prepared by co-precipitation and impregnation methods and used in dry reforming. The results illustrated that impregnated catalysts had higher particle size than precipitated ones after reduction because metal particles grow inside the pores in the precipitation methods while they grow on the surface of the support in impregnation method. The samples reduced at higher temperature had bigger particle size compared to those reduced at lower temperature. Bimetallic catalysts showed smaller particle size compared to monometallic ones.

5- It is also reported that the catalysts with higher Ni content showed better performance in the presence of H₂S because of better reduction of Ni compared to Co. It is also noted that the catalysts prepared by impregnation methods regenerated themselves better than precipitated ones due to

higher metal contents and reduction on the surface compared to precipitated catalysts. The bimetallic and Ni monometallic catalysts had higher resistance in the presence of steam than Co monometallic catalysts in dry reforming of biogas. Ni was reduced more than Co in both prepared samples with impregnation and co-precipitation (Shakouri, 2018)

6- The shaped NiCo catalysts, such as spherical catalysts and cylindrical/extrudate catalysts, prepared were stable and active for the DRM reaction during 800-900 °C with the strength similar to the commercial spherical alumina ones (Shakouri, 2018).

7- The CO₂ catalytic activation mechanism by considering the effects of contiguity of the two activation sites in the DRM was studied. In this regard, Ni in the NiM₂ (M₂=Co, Mn, Cu, and Fe) bimetallic MgO-spinel structure catalysts were prepared by co-precipitation method. The results demonstrated that the second metal affected the metallic particle sizes as well as basicity of the catalysts. Furthermore, it is reported that stronger basic sites were related to MgO solid solution phase, where metallic sites preferred to sit for the catalysts with various Mg contents. The smaller particles also created more chance for the activated reactant on metallic sites to reach the other reactant activated on the basic sites around it, as well as good contiguity of metallic and basic sites, thus leading to higher activities (Gao et al., 2020).

Chapter 3. Research Methodology

In this chapter, catalysts preparation methods, experiment set-up, and characterization techniques are described in detail.

3.1. Catalyst preparation methods

In this study, two catalysts preparation methods were used, impregnation for the supported catalysts and microemulsion for the core-shell structure catalysts.

Supported catalysts: Commercial γ - Al_2O_3 (Alfa- Aeser, Massachusetts, USA) was impregnated with aqueous solution of $\text{Ni}(\text{NO}_3)_2$ with appropriate concentration to obtain 5%, 12%, and 20 wt. % Ni content (0.198, .476, and 1.58 g of $\text{Ni}(\text{NO}_3)_2$, respectively). Afterward, the obtained solution was dried at 80 °C overnight and calcined for 3 h at 750 °C in air with the rate of 1°C/min and $\text{Ni}/\text{Al}_2\text{O}_3$ was prepared as the supported catalyst.

The schematic of catalysts preparation method is shown in Figure 3.1.



Figure 3.1. Schematic of catalysts preparation method as the supported catalyst

Core shell catalyst: The core shell catalysts were prepared with the microemulsion method. In this method, cyclohexane, polyoxyethylene cetyl ether and nickel nitrate were used as an oil phase, surfactant, and water phase, respectively. First, appropriate amount of surfactant (8.4, 20.1, and 33 g) and cyclohexane (200, 480, and 800 ml) were dissolved and then appropriate amount of nickel nitrate (0.198, .476, and 1.58 g) was added. After 10 h stirring, hydrazine (0.18, 1.8, and 1.1 ml) was added as a precipitating agent and alumina isopropoxide ($\text{C}_6\text{H}_{21}\text{O}_3\text{Al}$) (1.07, 2.58, and 4.3 g)

was added as a shell precursor to obtain catalysts with 5%, 12% and 20 wt. % Ni loadings, respectively. The prepared solution was stirred for about 24 h, dried at 45 °C vacuum oven and calcined at 750 °C in air for 3 h with the rate of 1 °C/min and Ni@Al₂O₃ catalyst was prepared with the core shell structure.

Schematic of catalysts preparation method is shown in Figure 3.2.

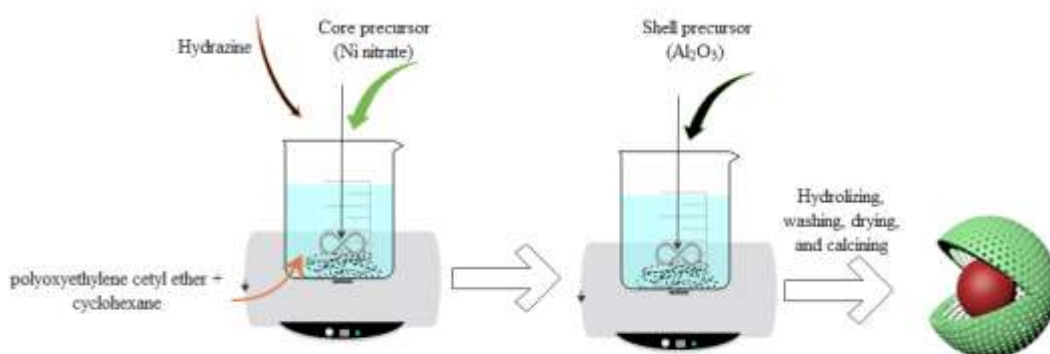


Figure 3.2. Catalyst preparation method with microemulsion method

3.2. Characterization techniques

Various characterization methods were used to analyze and study the catalysts activity and stability in dry reforming of methane, described in the following:

Brunauer–Emmett–Teller (BET) Surface Area Analysis

This technique is used to study structural properties of the catalysts such as surface area, pore size distribution and pore volume of the catalysts. In this regard, N₂ adsorption/desorption analysis including automated gas adsorption analyzer (3Flex 3500, Micromeritics, Norcross, USA) was used. First, about 0.2 g of the catalysts were degassed for 60 min at 90 °C followed by heating to 350 °C for 4 h by using a VacPrep system (Micromeritics).

X-ray diffraction (XRD) Analysis

In this technique, employed to study the crystallinity of the catalysts, Cu K α radiation on Bru-ker Advance D8 series II, and powder diffractometer was used. The diffraction spectra were collected in the range of 2 θ = 10-80 and Scherer equation was used to measure crystalline size of the catalysts.

Temperature-programmed reduction (TPR) analysis

TPR analysis is used to evaluate reducibility of the catalysts. Micromeritics AutoChem HP instrument, Norcross, USA was used for this purpose. The samples were heated up to 800 °C with ramp rate of 10 °C/min, using 10 % H₂ in Argon with 50 ml/min flow rate and the spectra were collected.

H₂ chemisorption

Micromeritics ASAP 2020, Norcross, USA equipment was used to determine dispersion of active metals on the catalysts. In this method, dispersion was measured in the presence of H₂ at high temperature.

Transmission Electron Microscopy (TEM)

Morphology of the catalysts was determined by TEM analysis, using a Hitachi HT7700 instrument at a magnification of 150 k at 100 kV accelerating voltage.

X-ray Photoelectron Spectroscopy (XPS)

In order to study the surface of the catalysts, XPS analysis was employed by using Kratos (Manchester, UK) AXIS Supra system, equipped with 500 mm Rowland circle monochromated Al K- α (1486.6 eV) source, combined hemi-spherical analyzer (HSA), and spherical mirror analyzer (SMA). A spot size of hybrid slot of 300x700 microns was used. All survey scan spectra were collected in the 5-1200 binding energy range in 1 eV steps with a pass energy of 160 eV.

X-ray absorption spectroscopy (XAS)

The XAS was carried out for the reduced catalysts at Canadian Light Source, Saskatoon, Saskatchewan. First all catalysts were reduced in presence of H₂:N₂= 40:60 at 750 °C for 3 h before analysis. Then the reduced samples were dispersed on a sample holder in a glove box under nitrogen. The catalysts were analyzed at Soft X-Ray Microcharacterization Beamline (SXRMB) beamline. The Ni K-edge absorption spectra were collected in total electron yield. Athena software was also used to analyze the data.

Inductively coupled plasma (ICP)

This method was used to measure the amount of active metal on the catalysts by using a Sciex Elan 5000 ICP-MS (PerkinElmer, USA). In this technique, the fresh catalysts were added to HCl/HNO₃ 3:1 solution following by addition of water to 0.5 ml of solution to obtain 10 ml of total in volume. Then, a 0.2 µm hydrophobic filter was used to filter the solution.

Carbon, Hydrogen, Nitrogen, Sulfur (CHNS) Analysis

In order to measure the amount of carbon deposited during the reaction, a VarioEL Cube (Elementar, Ronkonkoma, USA) device was used. This device was employed to measure the elements of carbon, hydrogen, nitrogen, and sulfur on the surface of the catalysts.

3.3. Experimental set-up for DRM reaction

The equipment used for this study include mass flow controller, catalytic activity up measurement set-up, and gas chromatograph which are described in the following.

Mass Flow Controller (MFC)

Mass flow controller (Brook instrument) is used to set and measure the gas stream. This instrument can measure the gas stream between 0 to 1000 ml/min.

Experimental set-up for evaluation of catalysts' activity

Figure 3.3 shows the schematic set-up used for the investigation of catalysts activity and stability in dry reforming of methane. In this set-up, 50 mg of the prepared catalyst was sieved with No. 60 sieve (U.S.A. standard testing sieve) to have uniform particles and mixed with 450 mg silica carbide and loaded in the quartz fixed- bed reactor with length of 300 mm and diameter of 5 mm. The temperatures of catalyst bed and reactor wall were measured with two K- type thermocouples which were inserted in the middle and wall of the reactor, respectively. At first, the catalysts were reduced with 100 ml/min stream of N₂:H₂ (60:40) by heating up to 750 °C at 5 °C/min ramp at 3 h. Then, N₂, CH₄ and CO₂ (N₂:CH₄:CO₂=1:1:1; GHSV= 144 L. g⁻¹. h⁻¹) were passed through the catalyst while the temperature kept at 750 °C for 5 h and 24 h to carry out short and long term dry reforming reaction tests, respectively. The outlet of the reactor was connected to the gas chromatograph to analyze the effluent gases. After the reaction, the used catalysts were cooled

down to the room temperature in the presence of Ni and samples were collected for further analyses.

The equations used for calculation of conversion, and reaction rate are shown in the following:

$$\text{CH}_4 \text{ conversion (\%)} = \frac{F_{in\text{CH}_4} - F_{out\text{CH}_4}}{F_{in\text{CH}_4}} * 100 \quad (3-1)$$

$$\text{CO}_2 \text{ conversion (\%)} = \frac{F_{in\text{CO}_2} - F_{out\text{CO}_2}}{F_{in\text{CO}_2}} * 100 \quad (3-2)$$

$$-r_{\text{CH}_4} = \frac{F_{in\text{CH}_4} - F_{out\text{CH}_4}}{m_{\text{catalyst}}} \quad (3-3)$$

$$-r_{\text{CO}_2} = \frac{F_{in\text{CO}_2} - F_{out\text{CO}_2}}{m_{\text{catalyst}}} \quad (3-4)$$

Where F and m represent flow rate and catalyst weight, respectively.

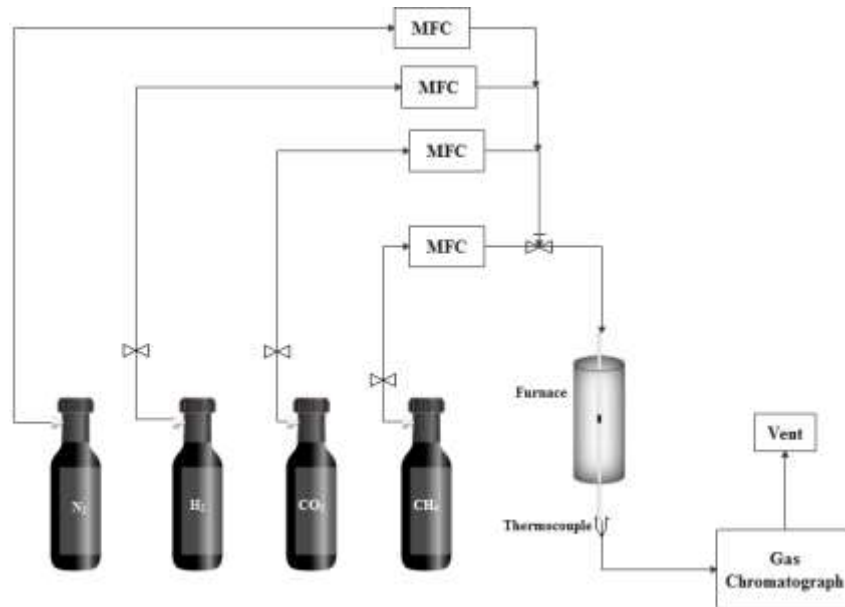


Figure 3.3. Schematic of set-up used for study of activity test

Gas chromatograph (GC)

Gas chromatograph (Agilent Technologies, 6890N) is used to analyze the effluent gases from the reactor with thermal conductivity detector (TCD).

Chapter 4. Results and Discussion

This chapter includes the results obtained from the catalysts' characterization and catalytic activity test in DRM in detail.

4.1. Structural properties of the catalysts

N₂ adsorption/desorption analysis is shown in Figure 4. 1. As it is observed in Figure 4. 1 a, all the catalysts have IV type isotherm, indicating mesopores structure with H2 shaped hysteresis loop which generally illustrates cylindrical-shaped channels with non-uniform pores (Alipour et al., 2014c). Moreover, based on the Figure 4. 1 b, pore size distribution of the supported and core shell structure catalysts show that the pore size is in the range of 3-4 nm for all the catalysts but core shell catalysts have smaller pore size, indicating their higher BET surface area. Further, based on Table 4. 1, BET surface area of the catalysts illustrated that core shell catalysts have higher BET surface area than supported catalysts, indicating better dispersion and more available active site with smaller particle size for these type of catalysts. Additionally, pore width in core shell structure catalysts is smaller than supported ones. The crystal size of NiO in the supported catalysts increased by increasing Ni loading while there is no change in this factor in the core shell catalysts due to encapsulation of NiO with alumina, resulting to lower agglomeration of Ni during calcination. Totally, core-shell structure catalysts showed higher BET surface area, pore volume with smaller pore diameters, resulting to better dispersion of Ni with smaller particle size. This come from encapsulation of Ni with alumina, inhibiting Ni from agglomeration during calcination. As a result, better catalytic performance is expected for the core-shell catalysts than the supported catalysts (Kang et al., 2011; Huang et al., 2017).

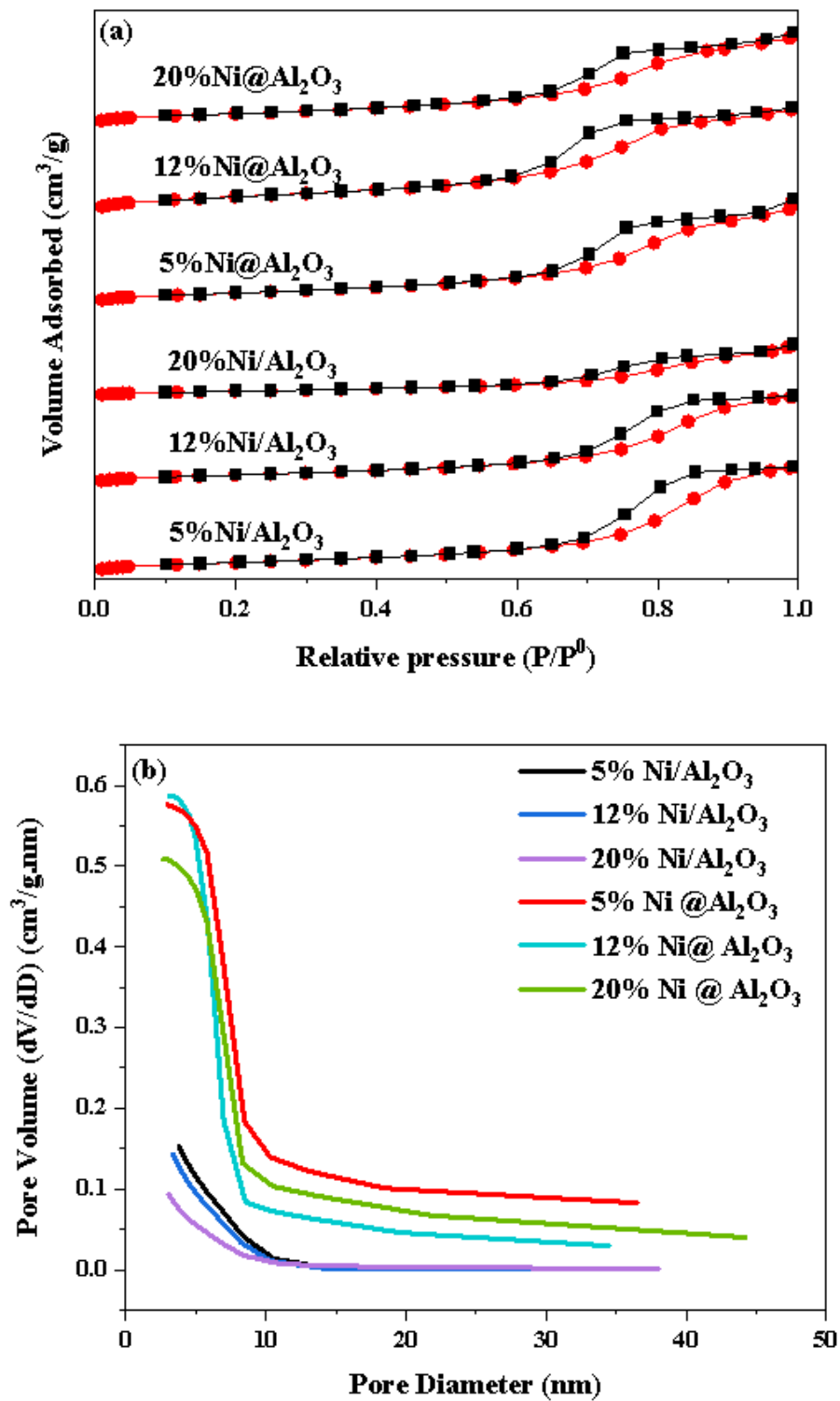


Figure 4.1. (a) N_2 adsorption/ desorption isotherm (b) Pore size distribution of Ni catalyst with supported and core- shell structure.

Table 4.1. Textural and structural properties of the catalysts.

Catalyst	S _{BET} ^a (m ² /g)	Pore volume ^b (cm ³ /g)	Pore width ^c (nm)	Crystal size of NiO ^d (Calcined) (nm)	Crystal size of Ni ^d (Reduced) (nm)
5%Ni/Al ₂ O ₃	193.00	0.60	8.6	4.2	-
12%Ni/Al ₂ O ₃	169.00	0.50	8.3	4.2	4.3
20%Ni/Al ₂ O ₃	97.00	0.30	9.0	5.0	-
5%Ni@Al ₂ O ₃	200.00	0.60	8.1	4.2	-
12%Ni@Al ₂ O ₃	282.00	0.60	6.6	4.3	4.2
20%Ni@Al ₂ O ₃	199.00	0.51	7.5	4.3	-

^a Calculated by BET equation

^b BJH desorption pore volume

^c BJH desorption average pore diameter

^d Crystalline diameter of NiO and Ni using Scherrer equation from XRD

XRD spectra of the fresh catalysts are shown in Figure 4. 2. NiO, NiAl₂O₄, and Al₂O₃ phases are observed in all catalysts. As it is seen, all three peaks detected for the core-shell catalysts, are assigned to NiO, NiAl₂O₄, and Al₂O₃ phases in the 2θ= 37.5°, 45.6°, and 66.5° in which the three detected phases are overlapped at 2θ=37.5° (Alipour et al., 2014c). Furthermore, there are three other peaks detected at 2θ= 43.74°, 63.38°, and 76° in the supported catalysts with 12 and 20% Ni, ascribed to NiO species. This is due to more available NiO in 12%Ni/Al₂O₃ and 20%Ni/Al₂O₃ catalysts with larger particle size while these two peaks are not detected in the core-shell catalysts due to better dispersion of NiO species with smaller particle size in these catalysts. Moreover, NiAl₂O₄ phase was detected for core-shell catalysts which was not detected for the supported catalysts. As can be seen, the peaks are sharper in the supported catalysts with higher Ni content due to more available Ni content. These peaks are not detected in the core-shell structured catalysts, indicating high NiO dispersion with smaller particle size in the core shell structured catalysts. Additionally, the catalysts with lower Ni loadings showed broader and narrower peaks, indicating better dispersion of Ni species. The intensity of the NiO peak increased with increasing Ni loading in the supported catalyst, indicating increased crystallinity of the NiO (Tian et al., 2022). To conclude, XRD spectra illustrated that NiO and NiAl₂O₄ species are the main phases in all prepared catalysts. The supported catalysts had sharper peaks due to larger particle size of NiO

compared to core-shell catalysts while more NiAl_2O_4 phase was detected for the core-shell catalysts.

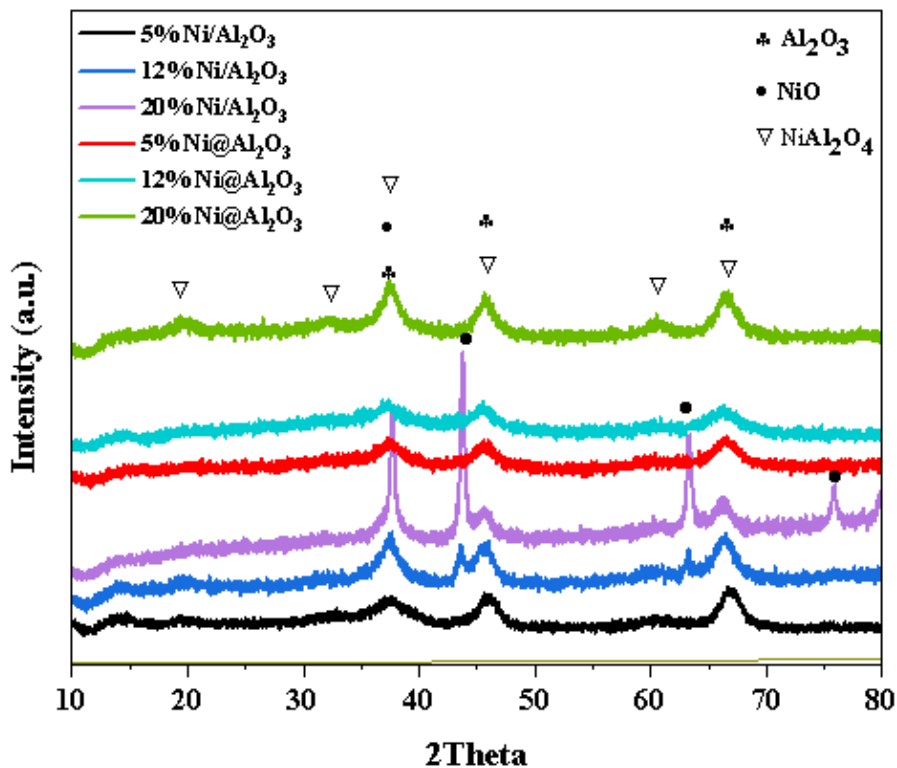


Figure 4.2. XRD patterns of calcined catalysts with the supported and core-shell structures

4.2. TPR analysis of the fresh catalysts

TPR results of the fresh catalysts with supported and core-shell structures are shown in Figure 4.3. NiAl_2O_4 peak is detected in all catalysts except for 20%Ni/ Al_2O_3 catalyst at high temperature between 600-800 °C, which showed strong interaction between Ni and Al_2O_3 . However, there are three main peaks in the 20%Ni/ Al_2O_3 catalyst at 338, 470, and 700 °C, assigned to NiO species with weak and strong interactions with the support and NiAl_2O_4 species, respectively (Alipour et al., 2014b). This can indicate that the catalyst with the supported catalysts with 5% and 12% Ni content and the core-shell catalysts with 5%, 12% and 20% Ni loadings had stronger Ni support interaction than the supported catalyst with the 20% Ni loading. As can be seen in the supported catalysts, the NiAl_2O_4 reduction peak is shifted to the lower temperature by increasing Ni loading,

which is due to lower Ni dispersion in the catalysts with higher amount of Ni loading, causing weaker interactions between Ni and support. In other word, there is stronger interaction between Ni and support in the 5% Ni/Al₂O₃ catalyst due to better dispersion and smaller particle size of Ni. Meanwhile, it can be seen that core-shell structured catalysts were reduced at lower temperature compared to the supported catalysts, showing that the core-shell structure improved catalyst reduction compared to the supported structure, which may be due to more area of Ni exposed to H₂ stream. It is obvious that the H₂ uptake is much higher in the core-shell structured catalysts compared to the supported catalysts, showing stronger interaction between Ni and alumina shell due to encapsulation of Ni with alumina, which has more surface area of Ni in contact with alumina in the core-shell type of catalysts (Li et al., 2019). Comparison of all the catalysts showed that 12% Ni@Al₂O₃ catalysts had better reducibility than other studied catalysts.

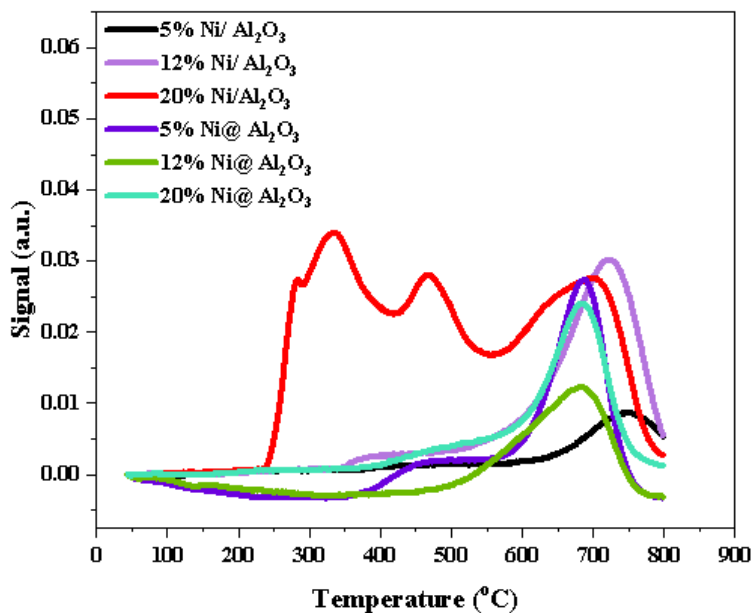


Figure 4.3. TPR spectra of the catalysts with the supported and core- shell structures

4.3. Morphology of the fresh catalysts with TEM and SEM analysis

The TEM analyses for the supported and core- shell structured catalysts with different Ni loadings are shown in Figure 4. 4. As can be seen, from Figure 4. 4a, b, and c, the core shell structure is successfully prepared. Further, the core shell structured catalysts have better dispersion with the smaller Ni particle size compared to the supported catalysts. Ni particles in the supported catalysts

have flake shape whereas Ni is covered with alumina in the core-shell structured catalysts. Additionally, it is observed from Figure 4. 5 that core-shell structured catalysts had smaller particle size (less than 10 nm) than the supported catalysts. This is due to better dispersion of Ni particles in the core-shell catalysts, encapsulated with alumina shell and decreased agglomeration of Ni particles. Further, the particle size increased by increasing the Ni loading in both types of catalysts due to more Ni contents and agglomeration of Ni particles on the catalysts.

The TEM images in this research are in good agreement with TEM images from literature in terms of core-shell structure. As shown in the Figure 4.6 a and b, Ni@Al₂O₃ and Ni/Al₂O₃ with the core-shell and supported structure were produced by Huang et al., (2017), respectively and it can be seen from Figure 4.6 c that Ni is covered with Al₂O₃ by Huang et al., (2017), which is similar with the Ni@Al₂O₃ produced (Figure 4.6 d) in this research.

SEM-EDS images of 12%Ni/Al₂O₃ and 12%Ni@Al₂O₃ catalysts are shown in Figure 4.7 a and b. The catalyst with core-shell structure has more alumina in the EDS result and small amount of Ni could be detected, indication encapsulation of Ni with alumina which EDS could not detect Ni while in the supported catalysts, more Ni could be detected, may show the dispersion of Ni on the alumina.

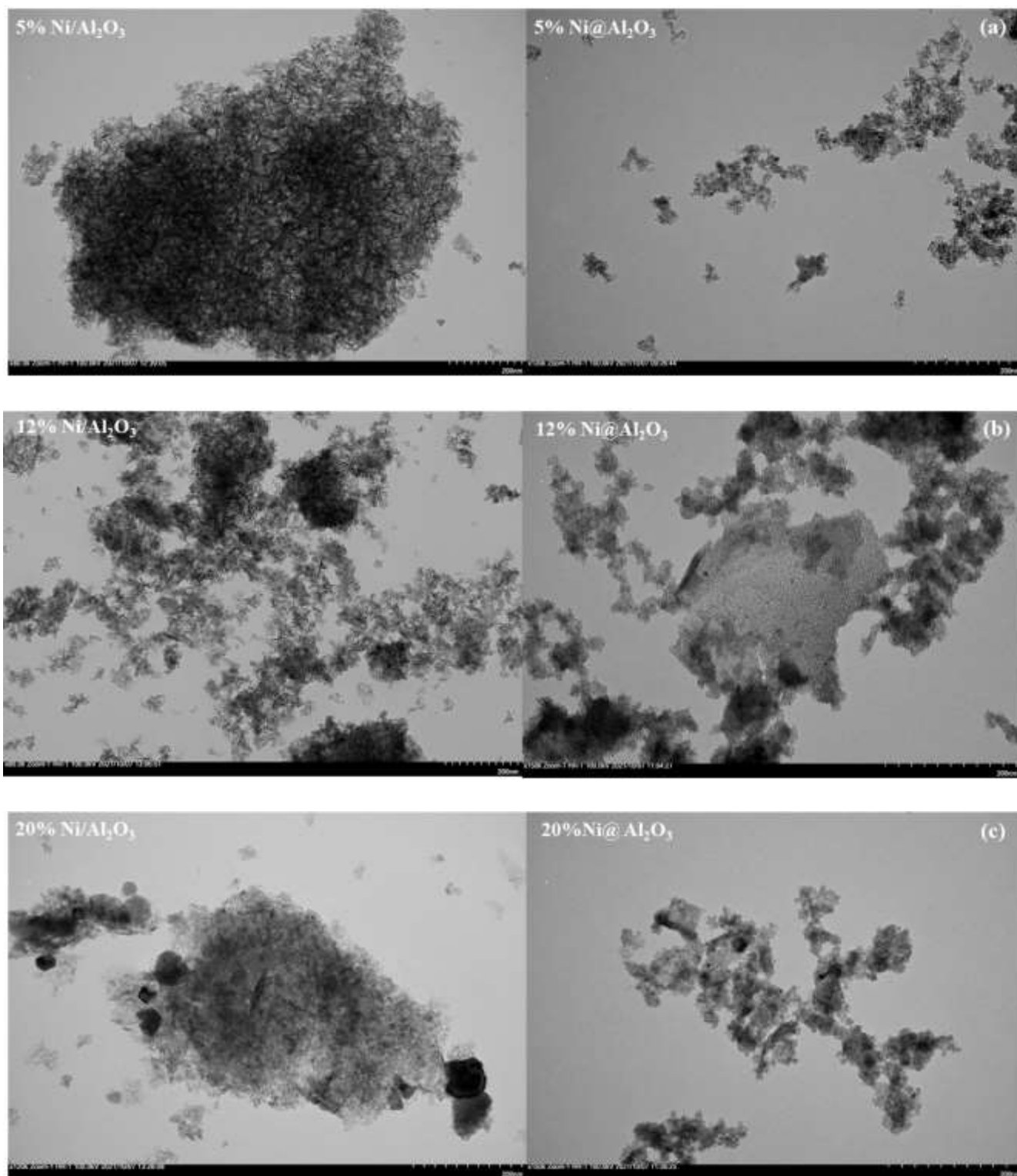


Figure 4.4. TEM analysis of the fresh supported and core-shell structure catalysts

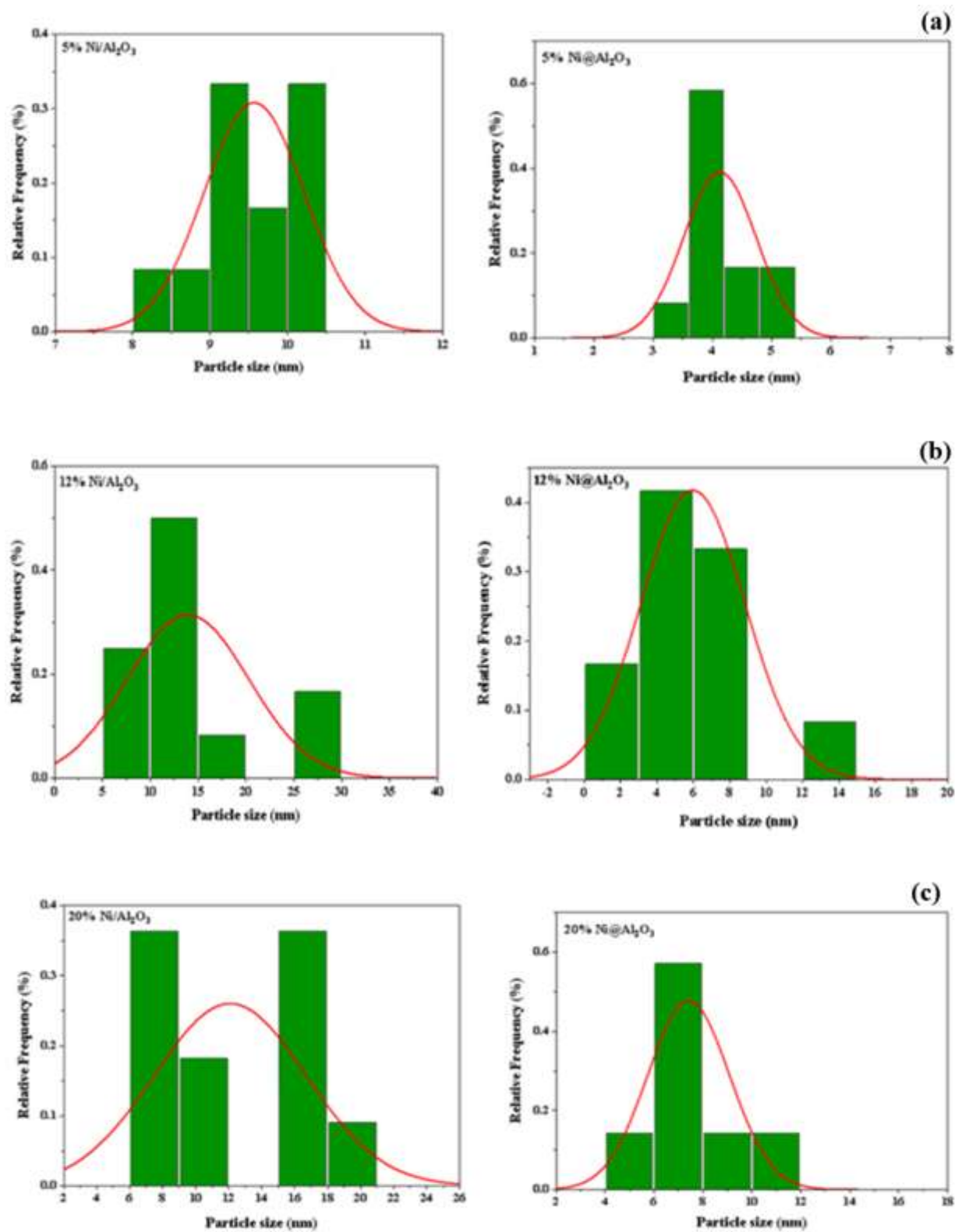


Figure 4.5. Particle size distribution of the fresh catalysts with the supported and core-shell structures

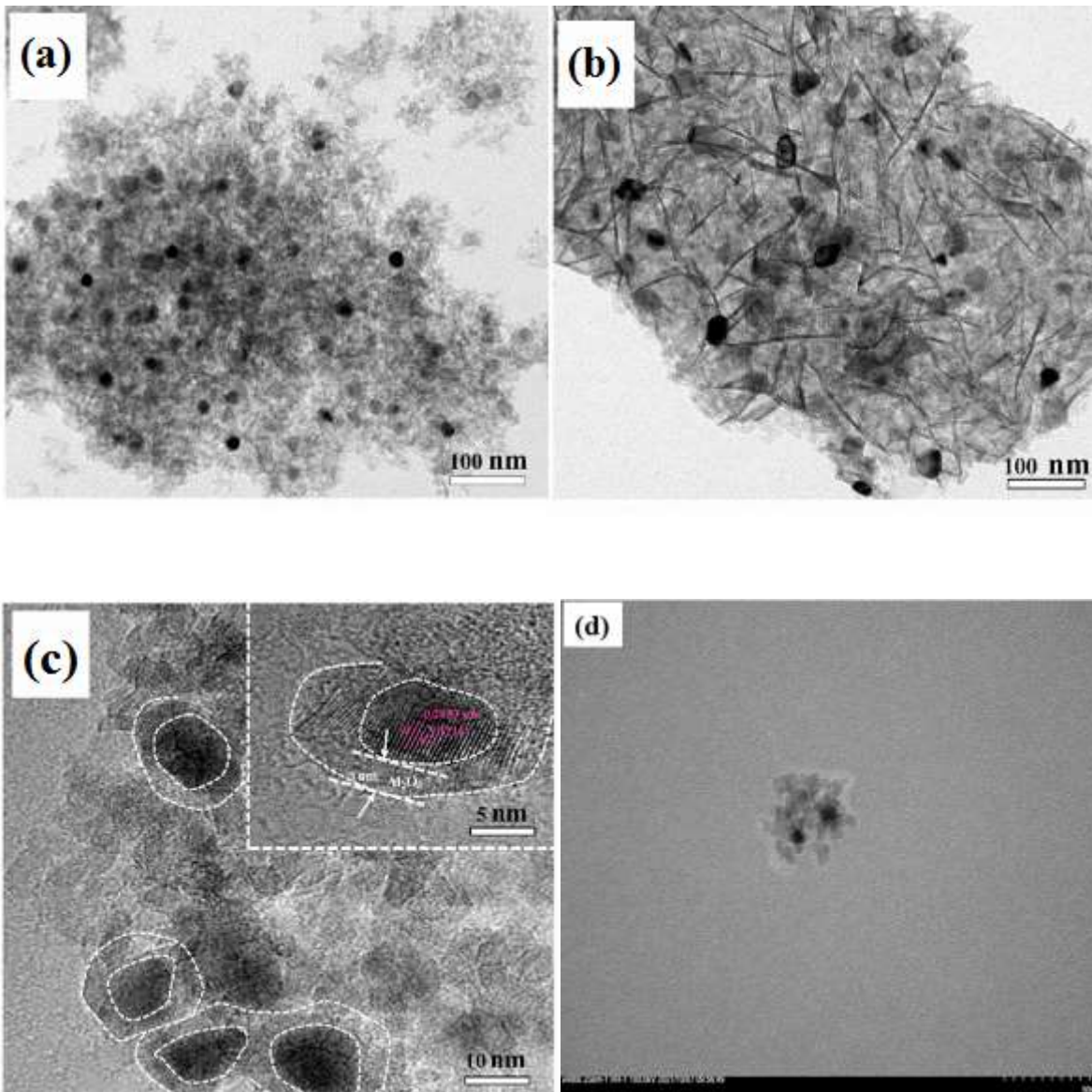


Figure 4.6. TEM images of Ni alumina with the core shell and supported structures in other literature (a) Ni@Al₂O₃ (b) Ni/Al₂O₃ (c) Ni@Al₂O₃ with high resolution (d) Ni@Al₂O₃ in this research (Huang et al., 2017)

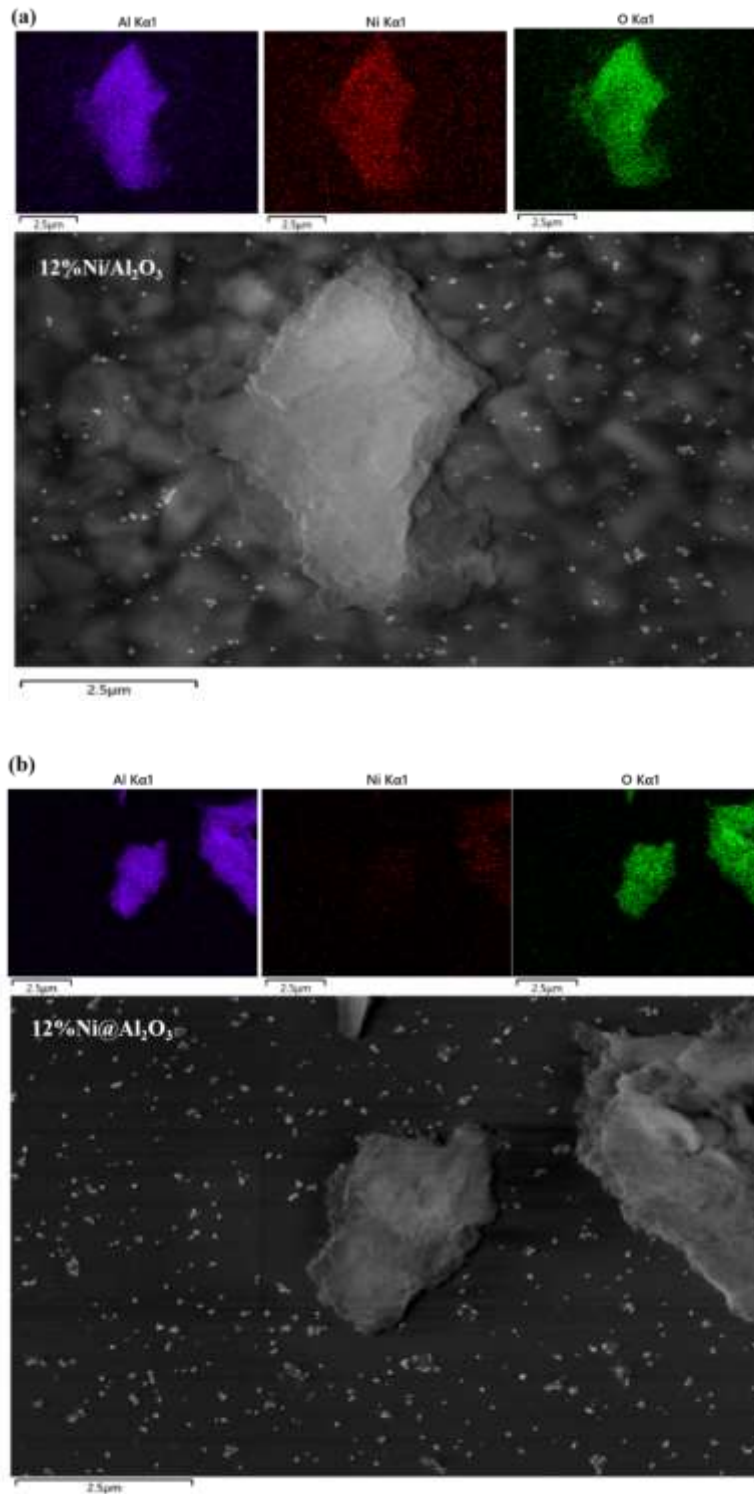


Figure 4.7. SEM-EDS images of calcined (a) 12%Ni/Al₂O₃ and (b) 12%Ni@Al₂O₃ catalysts

4.4. XPS analysis

XPS spectra of the supported and core shell structured catalysts are shown in Figure 4. 8. As can be seen, all the catalysts have the same patterns with Ni 2p_{3/2} and Ni 2p_{1/2} peaks. As can be seen, Ni 2p_{3/2} peak showed binding energy (BE) of 853-854 ev for the supported catalysts, assigned to NiO species while Ni 2p_{3/2} at BE=856 ev peak is ascribed to NiAl₂O₄ species, which could be detected for core-shell catalysts due to more NiAl₂O₄ phase on the core-shell catalysts . (Yu et al., 2022). This is confirmed by XRD and TPR. Further, the intensity is higher for Ni 2p_{3/2}, in the supported catalyst with 20% Ni content due to more available NiO in this catalysts, confirmed by TPR analysis. It is also observed that core- shell structured catalyst slightly has higher binding energy (BE) compared to supported catalysts due to stronger interaction between Ni and alumina. By increasing the Ni contents, BE is decreased in all catalysts due to lower interaction between Ni and Al₂O₃. Since X-ray penetrated ~ 10 nm in the samples and Ni is covered with alumina in the core- shell catalysts, intensity of peaks are higher in supported catalysts compared to core shell structured catalysts. The Ni amount in bulk and surface structure is shown in Table 4. 2 for all the prepared catalysts. As it is seen, most of the Ni is in the bulk phase, which is measured by ICP analysis for the all samples. Furthermore, the amount of Ni amount on surface of the supported catalysts is higher than on the core-shell structured catalysts due to encapsulation of Ni with alumina shell and lower amount of Ni is contacted with X- ray in the XPS analysis.

Table 4.2. Bulk and surface amount of Ni

Catalysts	Bulk Ni wt.% (calculated by ICP)	Surface Ni wt.% (calculated by XPS)
5% Ni/Al ₂ O ₃	4.60	1.31
12% Ni/Al ₂ O ₃	11.20	2.05
20%Ni/Al ₂ O ₃	19.60	5.61
5%Ni@Al ₂ O ₃	4.80	1.09
12%Ni@Al ₂ O ₃	11.80	1.23
20%Ni@Al ₂ O ₃	20.10	1.22

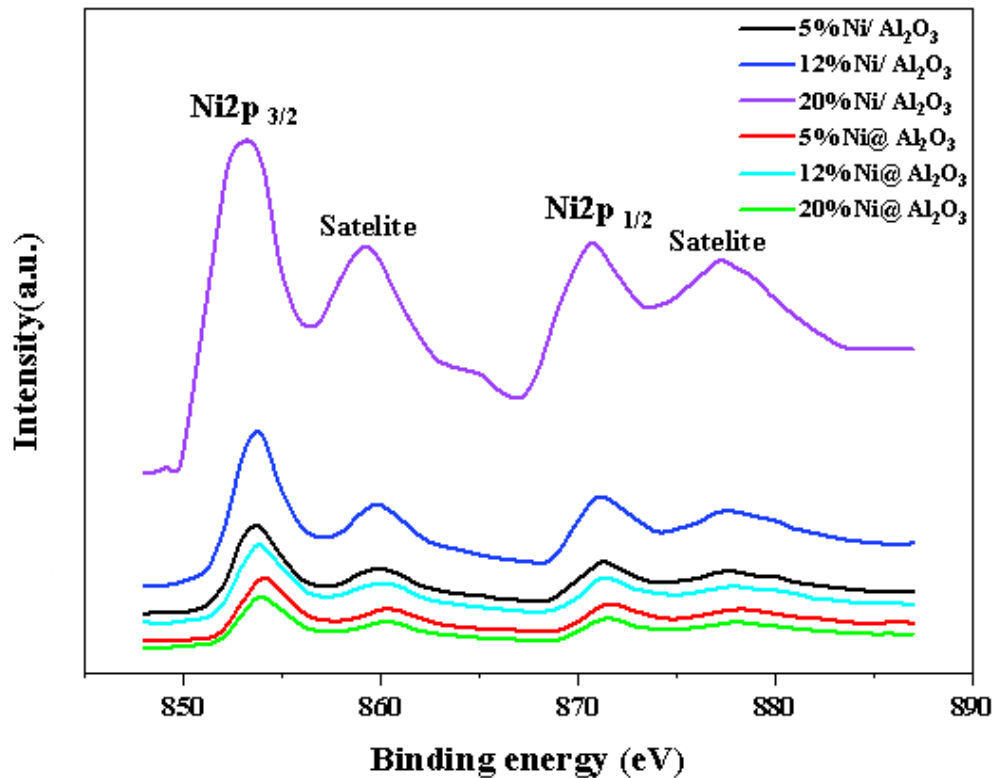


Figure 4.8. XPS spectra of supported Ni/Al₂O₃ and core- shell Ni@Al₂O₃

4.5. Study of reducibility of the catalysts

In order to compare the reduced and unreduced catalysts with the supported and core-shell structures, XRD and XAS spectra of the reduced catalysts were collected and are shown in Figure 4.9 and Figure 4.10, respectively. For XRD analysis, catalysts with 12% Ni loading with the supported and core-shell structures are chosen. As it is seen, Al₂O₃ and Ni species are detected in all catalysts, showing the good reduction of NiO and NiAl₂O₄ species into Ni species and presenting adequate active sites for reaction. Furthermore, the Ni species peak is sharper in the reduced catalysts than NiO and NiAl₂O₄ species peaks in unreduced catalysts. This shows better crystallinity in the reduced catalysts in the presence of H₂ stream. The crystal size of the reduced catalysts is calculated and presented in Table 4.1. As it can be seen, the crystal size is larger in the reduced catalysts than unreduced catalysts due to agglomeration of Ni particles during reduction. However, there is small change in the crystal size of the Ni species in the core-shell structured catalysts compared to the supported catalysts due to encapsulation of Ni species within the alumina

shell, leading to decrease in Ni movement at high temperature. It is noteworthy to mention that the peaks assigned to Ni species in the reduced catalysts are broader in the core-shell structure catalysts than in the supported catalysts. This can be explained by Scherrer equation that the catalysts with broader peak has higher FWHM (Full Width at Half Maximum) which is inversely proportional with crystal size. So, 12% Ni@Al₂O₃ catalysts has smaller crystal size than 12% Ni/Al₂O₃ catalysts. The catalysts with smaller crystal size has smaller particle size with better dispersion which leads to better activity and lower amount of carbon deposition during dry reforming reaction.

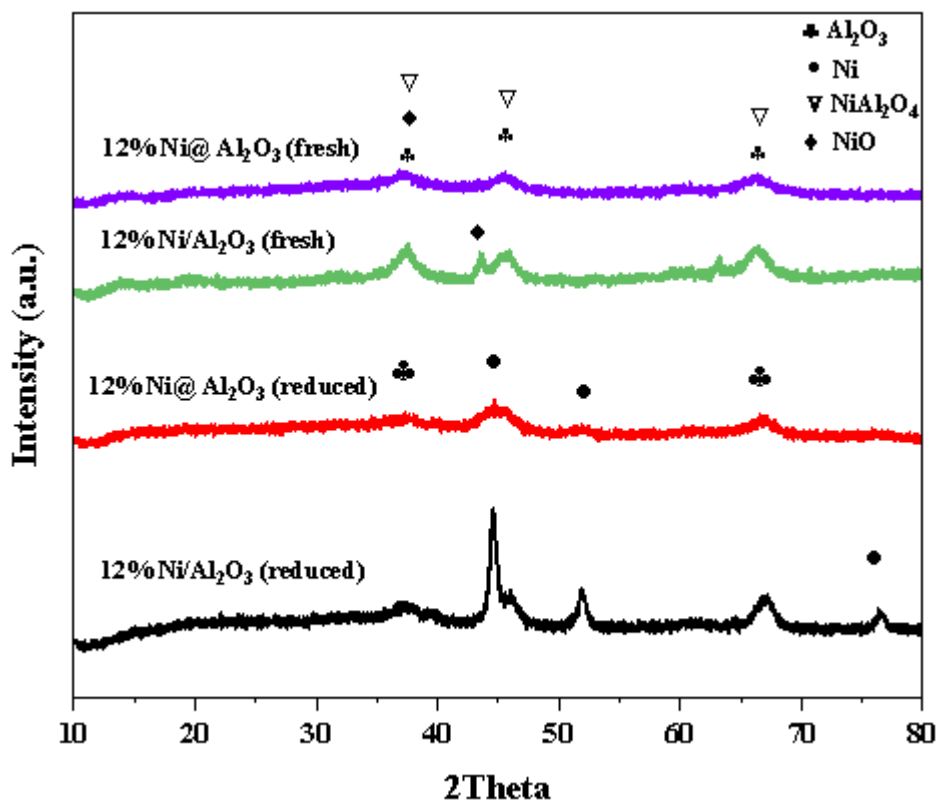


Figure 4.9. XRD patterns of reduced catalysts with 12% Ni loading with the supported and core-shell structures.

Ni K-edge X-ray Absorption Near Edge Spectroscopy (XANES) analysis was used to follow the reduction extent of Ni in the supported Ni/Al₂O₃ and core-shell Ni@Al₂O₃ catalysts with different

Ni loadings (5-20 wt.%). The reduction condition was temperature of 750 °C for 3 h in the presence of N₂:H₂= 60:40. The XANES spectra of the reduced catalysts, NiO standard and Ni foil are shown in Figure 4.10 a and b. As can be seen, all the catalysts reduced well and their spectra overlapped with Ni foil spectra. Further, XANES linear combination fitting is carried out to find out more quantitative information about the metal reduction extent. The fitting results for the reduced supported and core-shell structure catalysts were calculated with Athena software and are shown in Table 4.3. As can be seen, majority of NiO is reduced and adequate active sites are available for the reactant. Furthermore, supported catalysts have more Ni metal than the core-shell catalysts due to covering of metal with shell which causes less H₂ available for reduction while most of NiO are in the surface of the supported catalysts, making reduction easier. Another reason for this can be due to more NiAl₂O₄ species in the core-shell catalyst which causes a stronger interaction between Ni and alumina whereas supported catalyst with 20 % Ni is completely reduced due to more NiO species which confirmed by TPR results.

Table 4.3. Metal and metal oxide extent in reduced catalysts calculated by linear combination fitting of XANES. Reduction conditions were T= 750 °C for 3 h in H₂/N₂: 40/60

Catalyst	NiO (%)	Ni (%)
5% Ni/Al ₂ O ₃	10.00	90.00
12% Ni/Al ₂ O ₃	9.00	91.00
20% Ni/Al ₂ O ₃	-	100.00
5% Ni@Al ₂ O ₃	11.00	89.00
12% Ni@Al ₂ O ₃	20.00	80.00
20% Ni@Al ₂ O ₃	13.00	86.00

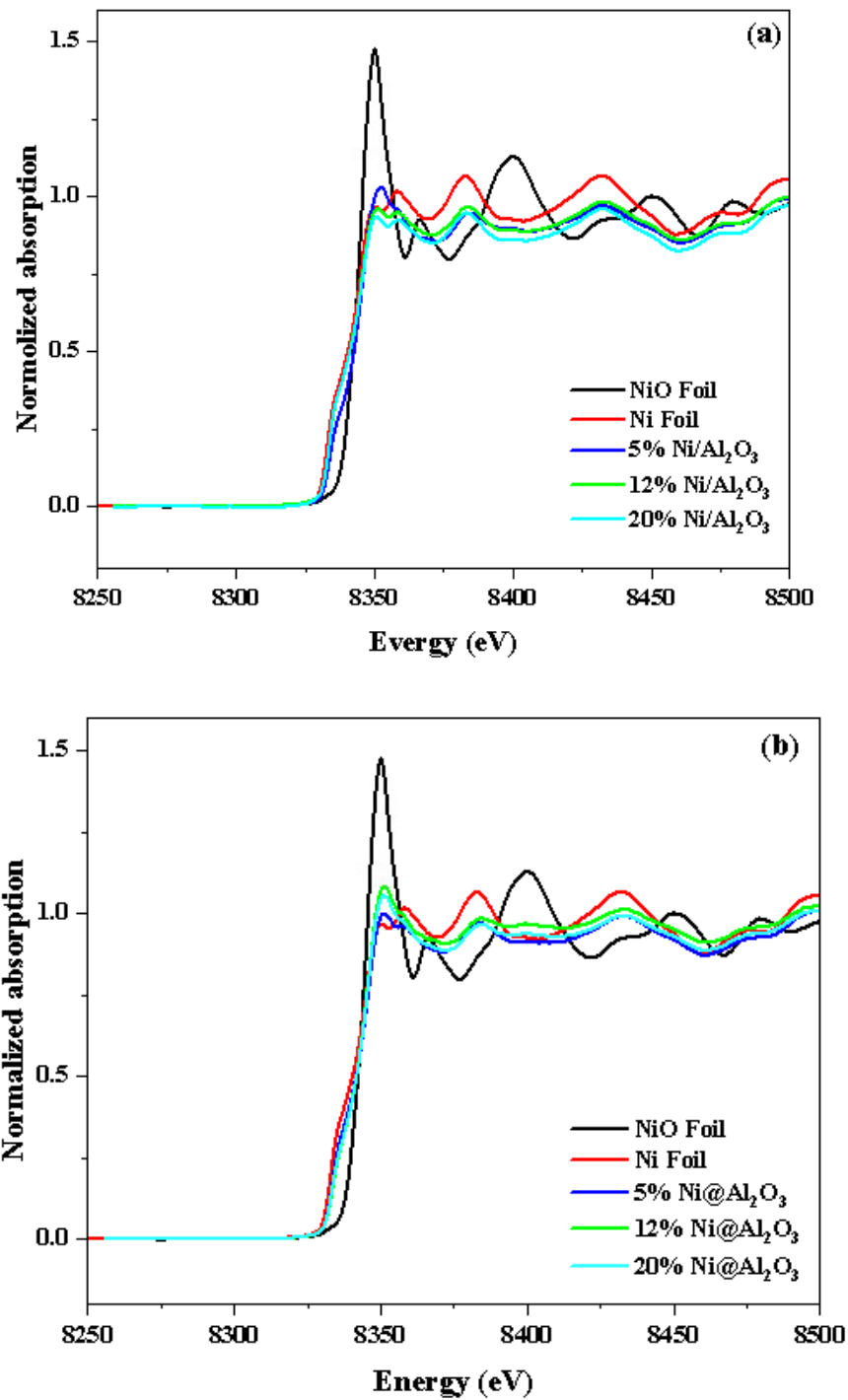


Figure 4.10. Ni K-edge XANES analysis of (a) supported and (b) core-shell structure catalysts reduced at 750 °C for 3 h in the presence of $N_2:H_2= 60:40$

TEM images and particle size distribution of the reduced catalysts are shown in Figure 4.11. First the samples were reduced in the presence of $H_2:N_2= 40:60$ at 750 °C for 3 h, and then TEM

analysis was used to see the impact of reduction on the morphology of the catalyst with the supported and core-shell structures. As can be seen, core-shell catalysts had smaller Ni particles compared to the supported catalysts due to better dispersion and encapsulation of Ni with outer shell. This indicates a lower amount of sintering in the core-shell catalyst after reduction in comparison to the supported catalysts. This results from encapsulation of Ni species with alumina shell in the core-shell catalysts which prevents Ni from agglomeration and sintering. Further, Figure 4.12 shows particle size distribution of Ni measured by TEM images for the reduced catalysts. As can be seen, it is confirmed that average particle size of Ni in the supported catalyst (more than 10 nm) are larger than the core-shell catalysts (less than 10 nm) due to encapsulation of Ni with outer shell.

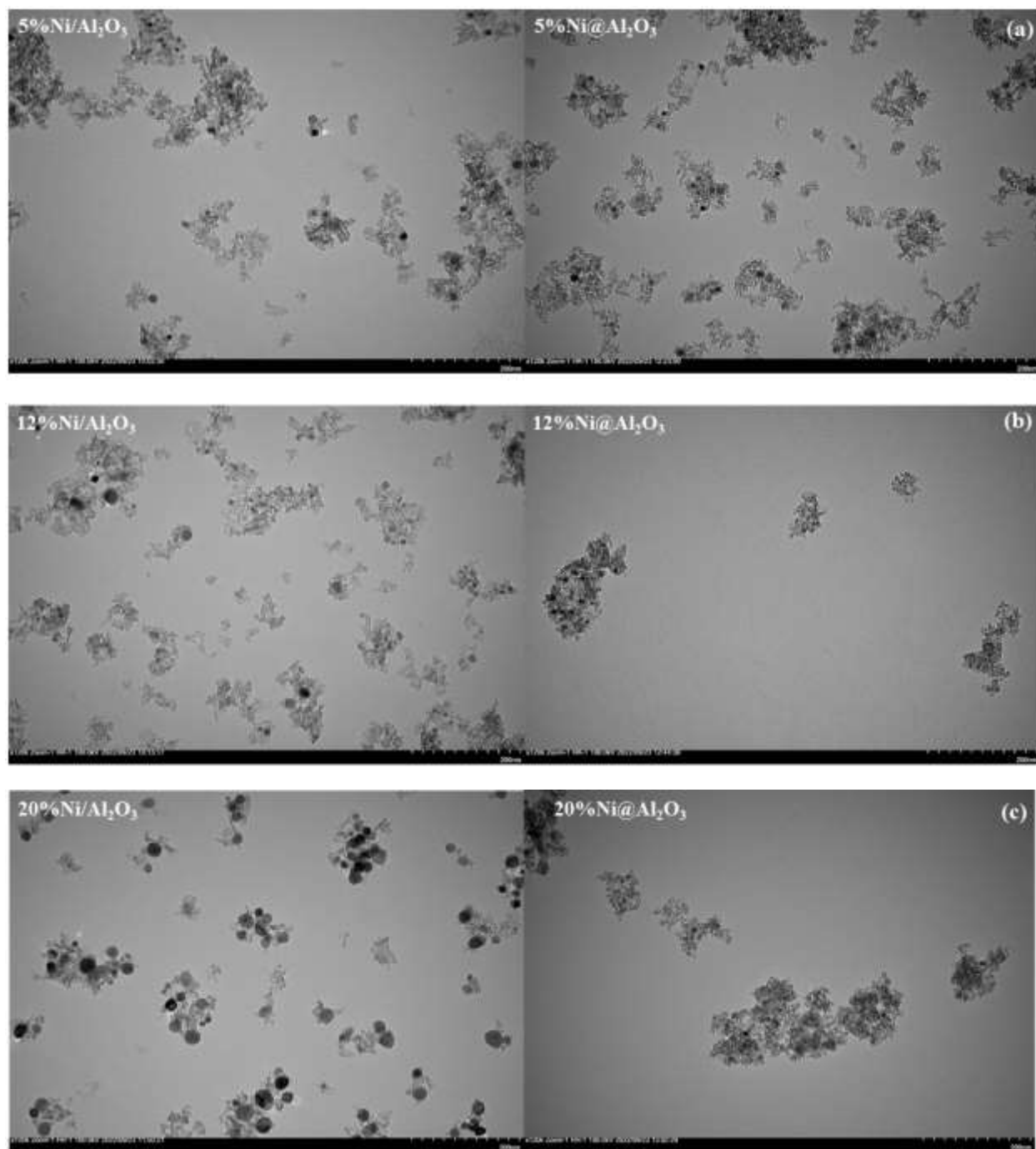


Figure 4.11. TEM analysis of of the reduced catalysts with the supported and core-shell structures

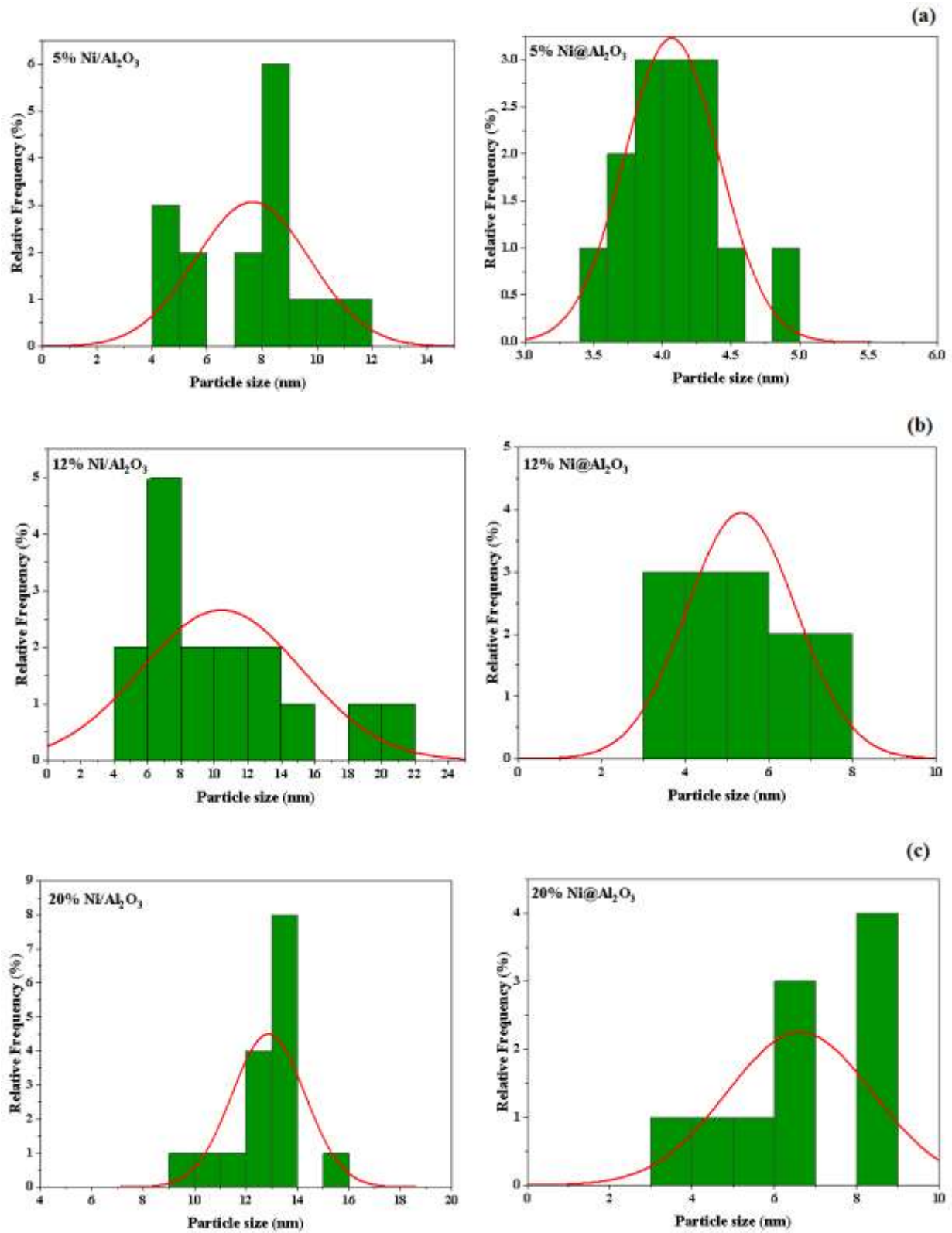
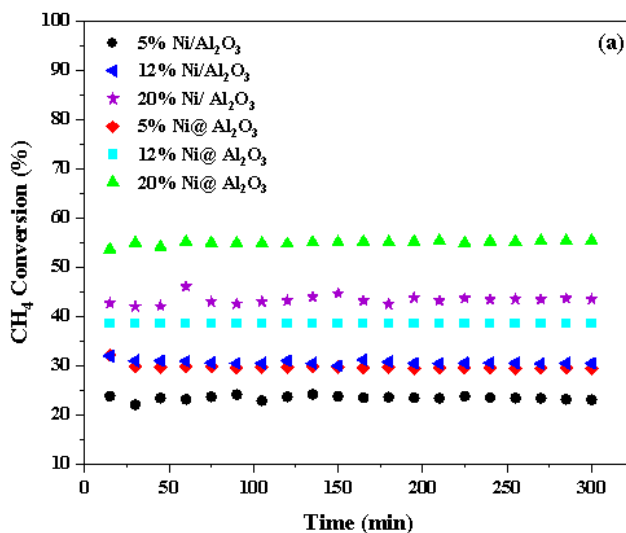
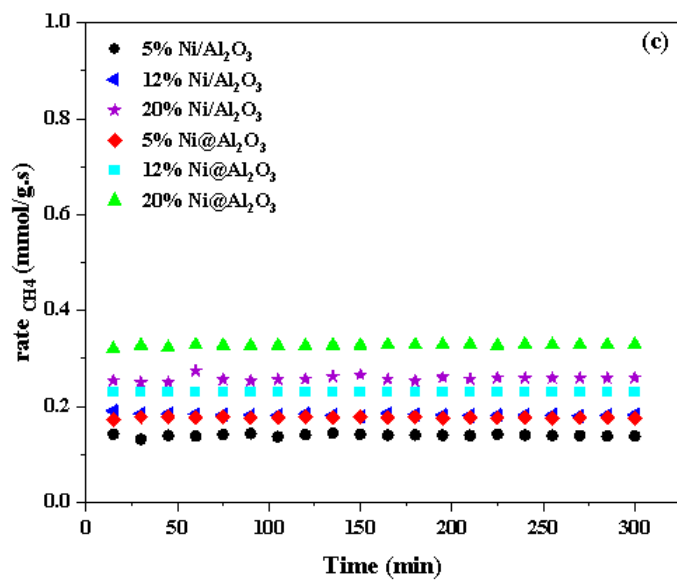
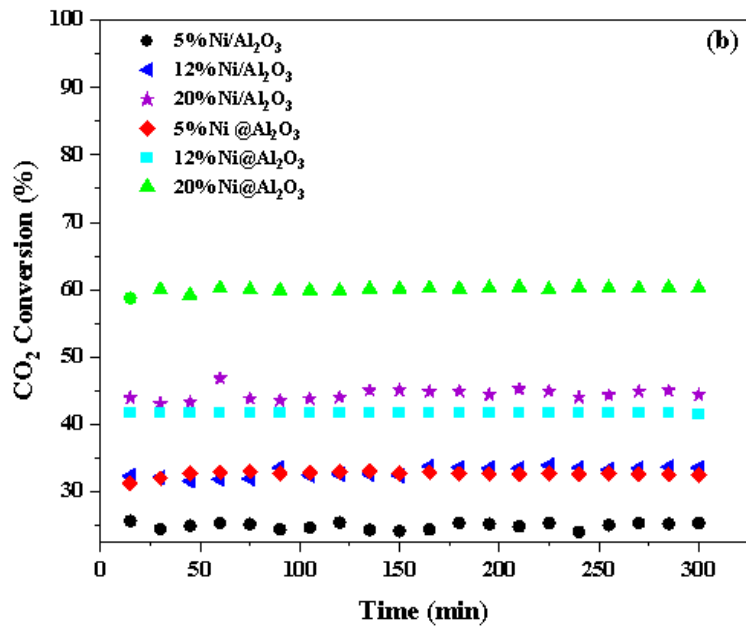


Figure 4.12. Particle size distribution of the reduced catalysts with the supported and core-shell structures

4. 6. Catalytic performance study

Dry reforming of methane is carried out in the presence of the prepared catalysts with the supported and core- shell structure at 750 °C, CH₄:CO₂:N₂=1:1:1, and GHSV= 144 (L.g⁻¹. h⁻¹) conditions and the results are shown in Figure 4. 13 as a function of CH₄ and CO₂ conversions, reaction rates, and H₂/CO ratio. As it is observed from Figure 4. 13 a and b, CO₂ conversion is higher than CH₄ conversion due to the reverse water-gas shift reaction (CO₂ + H₂ ↔ CO + H₂O), coming from reaction of produced H₂ with CO₂. The highest CH₄ and CO₂ conversion belongs to the catalysts with 20% Ni loading with the supported and core shell structures due to more available active sites for reaction. This trend is also seen for the reaction rate as well. Additionally, the core-shell structure catalysts displayed much higher reaction rate, conversion, and better catalytic activity compared to supported catalysts due to higher BET surface area, which provides more active sites for the reactants. Better dispersion of the Ni in the core shell structure catalysts significantly decreased Ni agglomeration and sintering and as a result increases the catalysts lifetime. The catalytic activity improved by increasing Ni content from 5 to 20 %, due to more available active sites for the reactants. From H₂/CO ratio graph (Figure 4. 13 e), it is observed that this ratio is less than 1 in all samples due to RWGS reaction. However, the 12%Ni@Al₂O₃ and 20%Ni@Al₂O₃ catalysts had H₂/CO ratio close to 1. This shows better catalytic performance of these two catalysts compared to other studied catalysts.





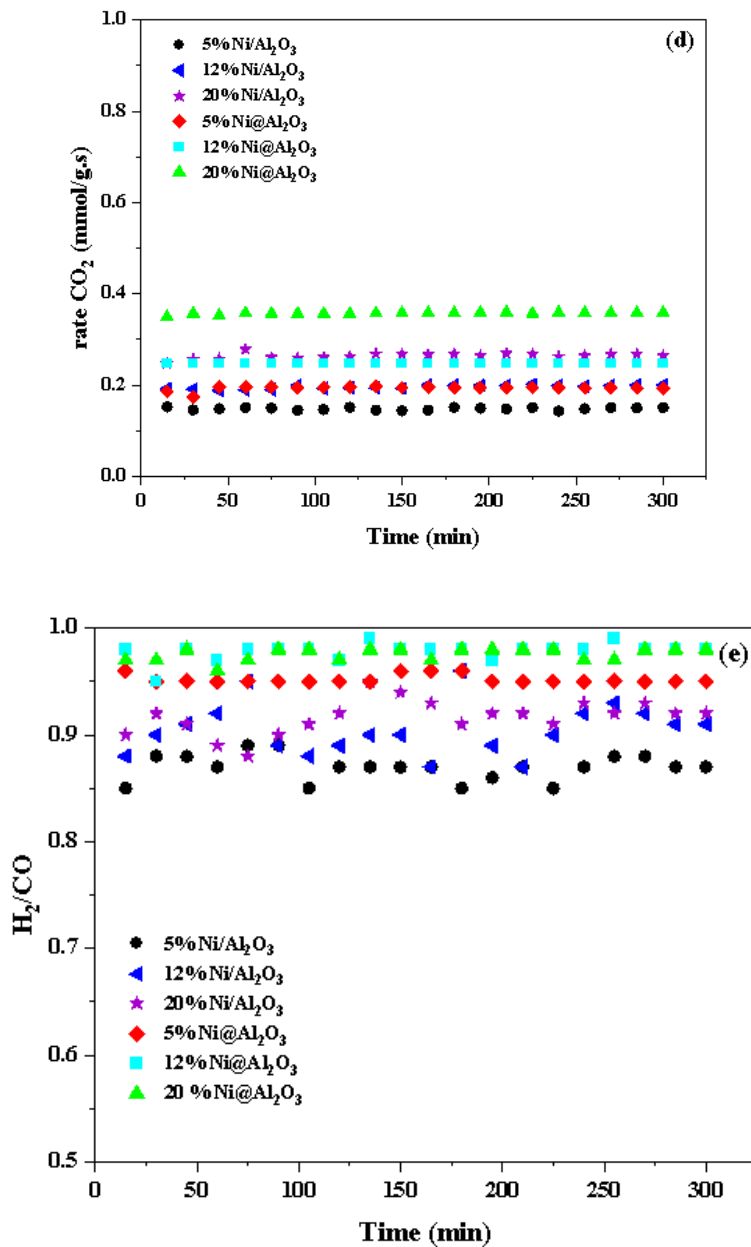


Figure 4.13. Catalytic reaction test over the supported and core-shell structures catalysts at 750 °C, CH₄:CO₂:N₂=1:1:1, GHSV= 144 (L.g⁻¹.h⁻¹), 5 h conditions. (a) CH₄ conversion, (b) CO₂ conversion, (c) rate (CH₄), (d) rate (CO₂), (e) H₂/CO ratio.

Based on the literature (Alipour et al., 2014a; Tavanarad et al., 2018), CH₄ and CO₂ conversions decline as GHSV increases due decrease in the residence time of reactant with the active site.

Comparison on the different catalysts with different GHSV are listed in the Table 4.4. As it is seen, the catalysts we prepared had great catalytic performance in DRM at high GHSV compared to other catalysts with low GHSV.

Table 4.4. Comparing different GHSV effect on the activity of the catalyst in DRM

Catalyst	GHSV (L.g ⁻¹ .h ⁻¹)	CH ₄ Con. (%)	CO ₂ Con. (%)	Reference
Ni@Al ₂ O ₃	144	54	60	This research
Ni/ Mg-Al ₂ O ₃	12	52	58	(Alipour et al., 2014b)
Ni@SiO ₂	18	50	60	(F. Wang et al., 2016)
Ni- CeO ₂ /MgO	18	35	68	(Khajenoori et al., 2015)
Ni-SiO ₂ @SiO ₂	24	72	94	(Kaviani et al., 2022)
Co/MgO	12	66	87	(Mirzaei et al., 2015)
Ni/MgAl ₂ O ₄	18	75	80	(Rezaei & Alavi, 2019)

4. 7. Carbon formation

Table 4. 5 shows the amount of carbon deposited on the core- shell and supported structured catalysts during dry reforming reaction, collected from CHNS analysis. As it is seen, the catalysts with 12% Ni have the lowest carbon deposition in the supported and core-shell structured catalysts and 12% Ni@Al₂O₃ has lower carbon deposition than 12% Ni/Al₂O₃ catalyst while it has higher catalytic activity. This may be due to lower Ni particle size and confinement effect within shell in the core-shell structured catalysts that leads to lower amount of carbon formation.

Table 4.5. The amount of carbon deposited from CHNS analysis

Catalyst	C (wt.%) (5 h reaction test)	C (wt.%) (24 h reaction test)	C (wt.%) (120 h reaction test)
5% Ni/Al ₂ O ₃	9.60±1.00	-	-
12% Ni/Al ₂ O ₃	5.30±1.00	-	-
20% Ni/Al ₂ O ₃	6.70±1.00	-	-
5% Ni@Al ₂ O ₃	5.80±1.00	-	-
12% Ni@Al ₂ O ₃	2.30±1.00	8.50 ±1.00	25.20±1.00
20% Ni@Al ₂ O ₃	5.30±1.00	-	-

XRD analysis of the used catalysts is shown in Figure 4. 14. It is seen that Al_2O_3 peak is observed in all samples while Ni species peak is detected only on the supported catalysts with 12 and 20% Ni loadings and the core-shell structured catalyst with 20% Ni content. This illustrates that Ni is still dispersed well in the supported catalyst with 5% and core shell catalysts with 5 and 12% Ni loadings. Furthermore, the peak assigned to Ni in the 20% $\text{Ni@Al}_2\text{O}_3$ catalyst is less sharp than in the 12% $\text{Ni/Al}_2\text{O}_3$ and 20% $\text{Ni/Al}_2\text{O}_3$ catalysts, due to agglomeration of Ni in the supported catalyst, which resulted in larger crystal size and sharper peak confirmed in XRD analysis compared to the core-shell structure catalyst during dry reforming reaction.

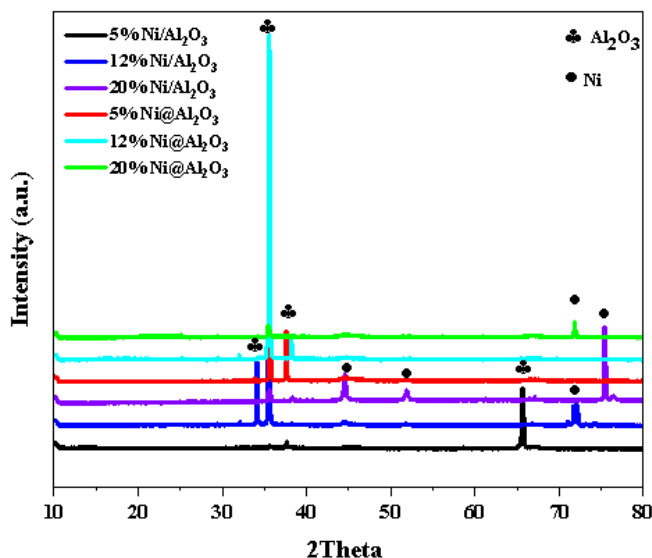


Figure 4.14. XRD analysis of the used catalysts after 5 h time on stream

Based on the catalytic activity and carbon formation results, it can be concluded that the 12% $\text{Ni@Al}_2\text{O}_3$ catalyst has the best catalytic performance and lower carbon formation in this reaction.

Long term stability test is carried out for 12% $\text{Ni@Al}_2\text{O}_3$ catalyst at 750 °C, $\text{CH}_4:\text{CO}_2:\text{N}_2=1:1:1$, and $\text{GHSV}=144\text{ (L.g}^{-1}.\text{h}^{-1})$ at 24 h and 120 h. The results are shown in Figure 4.15 a and b as a function of CH_4 conversion (%). As can be seen from Figure 4.15 a, the catalyst displayed great stability during 24 h time on stream with around 39 % methane conversion. It can be concluded that core-shell structure catalyst was incredibly stable during dry reforming reaction due to

encapsulation of Ni with alumina, which prevented Ni from agglomeration and sintering during the reaction. In addition, the 120 h stability test reaction showed bad stability during 120 h on stream from as the activity dropped from 39 % CH₄ conversion to around 12% CH₄ conversion. The CHNS results illustrated 25 % wt. carbon on the catalyst during the 120 h reaction which is much higher from the 5 h and 24 h stability tests which are 2.3 % and 8.5 %, respectively, as shown in Table 4.5. This shows that carbon was generated gradually, causing the catalyst deactivation during 120 h time on stream.

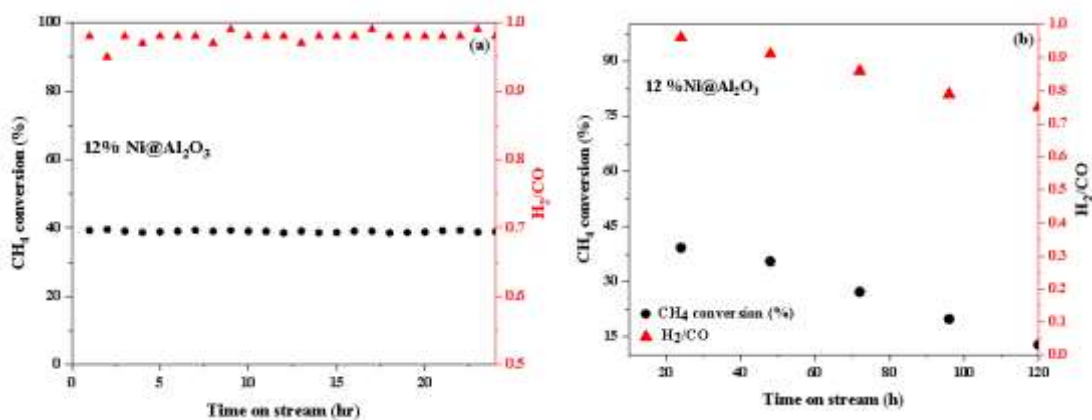


Figure 4.15. Long term catalytic stability test for 12% Ni@Al₂O₃ catalyst under 750 °C, (a) 24 h and (b) 120 h time on stream. CH₄:CO₂:N₂ = 1:1:1, GHSV = 144 (L.g⁻¹.h⁻¹), conditions (●) CH₄ conversion (▲) H₂/CO

Chapter 5. Conclusion and Recommendations

Since global warming has been harming our environment and changing the environment, many efforts are under way to overcome this issue. One of them is consuming two main greenhouse gases (CH_4 and CO_2) and convert them to the valuable chemical (syngas). Dry reforming of methane is one of the main processes in which methane and CO_2 are consumed and syngas (H_2/CO) is produced. The produced syngas is used in the production of other material such as methanol and Fischer-Tropsch synthesis. Coke formation and sintering are the main challenges in this reaction. Carbon is mainly deposited through CH_4 decomposition. There are many studies carried out to reduce the amount of carbon formation and prolong the catalyst lifetime such as using bimetallic nano-particles and providing more active sites for reactants, adding alkaline promoters to increase the basic properties of the catalysts. Core-shell structure catalysts is one the novel technique currently used to improve the catalytic performance in DRM. In this type of catalyst, the active metal is covered by shell and prevents it from moving and sintering. In this regard, core-shell structure catalyst is compared with supported catalyst in DRM in terms of catalytic activity and carbon formation. The main aim of this research was to increase the lifetime of catalyst in dry reforming of methane. In this regard, a novel $\text{Ni}@\text{Al}_2\text{O}_3$ catalyst with a core-shell structure was prepared with the microemulsion method and compared with the conventional $\text{Ni}/\text{Al}_2\text{O}_3$ catalyst with supported structure in DRM.

5.1. Conclusions

The structural properties of catalyst showed that core-shell catalysts had higher BET surface area with smaller pore size distribution due to encapsulation of Ni species with outer shell which prevents the active metals agglomeration during calcination. This results in better dispersion and smaller particle size of active metals. Furthermore, XRD analysis illustrated that more NiO phases were detected in the supported catalyst compared to the core-shell structure catalyst, indication better dispersion of NiO species with smaller particle size on the core-shell catalysts which could not be detected by X-ray. TPR results also displayed that core-shell structure catalysts reduced at lower temperature with lower amount of H_2 uptake compared to the supported catalysts. TEM analysis showed that core-shell structure catalysts were successfully prepared with smaller particle size distribution compared to the supported catalysts. XPS analysis also illustrated that NiO and NiAl_2O_4 species were the main available phases in the all catalysts. Furthermore, it showed that

core-shell catalysts slightly had higher binding energy than supported catalysts due to stronger interaction between Ni and alumina in this type of catalysts. XAS and XRD analysis were done for the reduced catalysts with 12 % Ni for the supported and core-shell catalysts. The results showed that all the NiO and NiAl₂O₄ species converted to Ni species during reduction. In addition, there is a small change in the crystal size of the reduced core-shell catalyst compared to the unreduced catalyst when it compared to the supported catalyst.

The catalytic activity test illustrated that core-shell catalysts had higher activity with lower carbon formation in dry reforming reactions. This results from encapsulation of Ni with alumina, preventing it from agglomeration and sintering. The XRD analysis for the used catalyst showed that Ni was still dispersed well in the core-shell structure catalyst while it might agglomerate in the supported catalysts.

The 24 h test showed great stability for the 12%Ni@Al₂O₃ catalyst in DRM. Furthermore, 5 days stability test was carried out for the 12%Ni@Al₂O₃ catalyst and the results showed gradual decline in the activity of the catalyst.

5.2. Recommendations

Some recommendation are summarized as follows for the future research work in dry reforming of methane:

- Reaction optimization for the core-shell catalysts should be carried out to find optimum GHSV, CH₄/CO₂ ratio, reaction, reduction and calcination temperatures on the catalytic activity and coke formation in this type of catalyst.
- Used catalysts should be studied in depth in order to find out how shell can protect active metal in dry reforming from agglomeration and sintering.
- Core-shell activity test should be done in the presence of impurities such H₂S, O₂, H₂O to find out how shell can protect the active metal from poisoning.
- The used core-shell catalysts should be regenerated and reused in DRM.
- In-situ characterization techniques should be used to identify what happens in the core-shell structure catalysts during the reduction and reaction such as XRD to find out crystalline size.
- Optimizing shell thickness should be studied and its effect on the catalytic activity and coke formation for the core-shell catalysts in DRM.

References

- Abatzoglou, N., & Fauteux-Lefebvre, C. (2016). Review of catalytic syngas production through steam or dry reforming and partial oxidation of studied liquid compounds. *Wiley Interdisciplinary Reviews: Energy and Environment*, 5(2), 169–187. <https://doi.org/10.1002/WENE.167>
- Aboonahr Shiraz, M. H., Rezaei, M., & Meshkani, F. (2016). Microemulsion synthesis method for preparation of mesoporous nanocrystalline γ -Al₂O₃ powders as catalyst carrier for nickel catalyst in dry reforming reaction. *International Journal of Hydrogen Energy*, 41(15), 6353–6361. <https://doi.org/10.1016/J.IJHYDENE.2016.03.017>
- Alabi, W. O. 1982-. (2018). *A STUDY OF STRUCTURAL PROPERTIES AND PERFORMANCE OF Ni-Co-Mg-Al-Ox CATALYST FOR CARBON DIOXIDE REFORMING OF METHANE*. <https://harvest.usask.ca/handle/10388/8474>
- Alipour, Z., Babu Borugadda, V., Wang, H., & Dalai, A. K. (2023). Syngas production through dry reforming: A review on catalysts and their materials, preparation methods and reactor type. *Chemical Engineering Journal*, 452, 139416. <https://doi.org/10.1016/J.CEJ.2022.139416>
- Alipour, Z., Meshkani, F., & Rezaei, M. (2016). Effect of K₂O on the catalytic performance of Ni catalysts supported on nanocrystalline Al₂O₃ in CO₂ reforming of methane. *Iranian Journal of Hydrogen & Fuel Cell*, 2(4), 215–226. <https://doi.org/10.22104/IJHFC.2016.264>
- Alipour, Z., Rezaei, M., & Meshkani, F. (2014a). Effect of Ni loadings on the activity and coke formation of MgO-modified Ni/Al₂O₃ nanocatalyst in dry reforming of methane. *Journal of Energy Chemistry*, 23(5), 633–638. [https://doi.org/10.1016/S2095-4956\(14\)60194-7](https://doi.org/10.1016/S2095-4956(14)60194-7)
- Alipour, Z., Rezaei, M., & Meshkani, F. (2014b). Effects of support modifiers on the catalytic performance of Ni/Al₂O₃ catalyst in CO₂ reforming of methane. *Fuel*, 129, 197–203. <https://doi.org/10.1016/j.fuel.2014.03.045>

- Alipour, Z., Rezaei, M., & Meshkani, F. (2014c). Effect of alkaline earth promoters (MgO, CaO, and BaO) on the activity and coke formation of Ni catalysts supported on nanocrystalline Al₂O₃ in dry reforming of methane. *Journal of Industrial and Engineering Chemistry*, 20(5), 2858–2863. <https://doi.org/10.1016/j.jiec.2013.11.018>
- Arora, S., & Prasad, R. (2016). An overview on dry reforming of methane: strategies to reduce carbonaceous deactivation of catalysts. *RSC Advances*, 6(110), 108668–108688. <https://doi.org/10.1039/C6RA20450C>
- Ay, H., & Üner, D. (2015). Dry reforming of methane over CeO₂ supported Ni, Co and Ni-Co catalysts. *Applied Catalysis B: Environmental*, 179, 128–138. <https://doi.org/10.1016/j.apcatb.2015.05.013>
- Aziz, M. A. A., Setiabudi, H. D., Teh, L. P., Anuar, N. H. R., & Jalil, A. A. (2019). A review of heterogeneous catalysts for syngas production via dry reforming. *Journal of the Taiwan Institute of Chemical Engineers*, 101, 139–158. <https://doi.org/10.1016/J.JTICE.2019.04.047>
- Bian, Z., Das, S., Wai, M. H., Hongmanorom, P., & Kawi, S. (2017a). A Review on Bimetallic Nickel-Based Catalysts for CO₂ Reforming of Methane. *ChemPhysChem*, 18(22), 3117–3134. <https://doi.org/10.1002/CPHC.201700529>
- Bian, Z., Das, S., Wai, M. H., Hongmanorom, P., & Kawi, S. (2017b). A Review on Bimetallic Nickel-Based Catalysts for CO₂ Reforming of Methane. *ChemPhysChem*, 18(22), 3117–3134. <https://doi.org/10.1002/CPHC.201700529>
- By, S., & Shakouri, M. (n.d.). *EFFECTS OF PREPARATION, Ni/Co RATIO, AND SULFURE POISONING OF Ni-Co BIMETALLIC CATALYST FOR DRY REFORMING REACTION.*
- Carapellucci, R., & Giordano, L. (2020). Steam, dry and autothermal methane reforming for hydrogen production: A thermodynamic equilibrium analysis. *Journal of Power Sources*, 469. <https://doi.org/10.1016/J.JPOWSOUR.2020.228391>
- Castro Luna, A., Becerra, A., Dimitrijewits, M., & Arciprete, C. (2000). Methane CO₂ reforming over a stable Ni/Al₂O₃ catalyst. *Studies in Surface Science and Catalysis*,

130 D, 3651–3656. [https://doi.org/10.1016/S0167-2991\(00\)80590-X](https://doi.org/10.1016/S0167-2991(00)80590-X)

- Chaudhary, P. K., Koshta, N., & Deo, G. (2020). Effect of O₂ and temperature on the catalytic performance of Ni/Al₂O₃ and Ni/MgAl₂O₄ for the dry reforming of methane (DRM). *International Journal of Hydrogen Energy*, 45(7), 4490–4500. <https://doi.org/10.1016/J.IJHYDENE.2019.12.053>
- Chein, R. Y., & Fung, W. Y. (2019). Syngas production via dry reforming of methane over CeO₂ modified Ni/Al₂O₃ catalysts. *International Journal of Hydrogen Energy*, 44(28), 14303–14315. <https://doi.org/10.1016/J.IJHYDENE.2019.01.113>
- da Fonseca, R. O., Garrido, G. S., Rabelo-Neto, R. C., Silveira, E. B., Simões, R. C. C., Mattos, L. V., & Noronha, F. B. (2020). Study of the effect of Gd-doping ceria on the performance of Pt/GdCeO₂/Al₂O₃ catalysts for the dry reforming of methane. *Catalysis Today*, 355, 737–745. <https://doi.org/10.1016/J.CATTOD.2019.04.079>
- Damyanova, S., Pawelec, B., Arishtirova, K., Huerta, M. V. M., & Fierro, J. L. G. (2009). The effect of CeO₂ on the surface and catalytic properties of Pt/CeO₂–ZrO₂ catalysts for methane dry reforming. *Applied Catalysis B: Environmental*, 89(1–2), 149–159. <https://doi.org/10.1016/J.APCATB.2008.11.035>
- Das, S., Lim, K. H., Gani, T. Z. H., Aksari, S., & Kawi, S. (2022). Bi-functional CeO₂ coated NiCo-MgAl core-shell catalyst with high activity and resistance to coke and H₂S poisoning in methane dry reforming. *Applied Catalysis B: Environmental*, 122141. <https://doi.org/10.1016/J.APCATB.2022.122141>
- Dekkar, S., Tezkratt, S., Sellam, D., Ikkour, K., Parkhomenko, K., Martinez-Martin, A., & Roger, A. C. (2020). Dry Reforming of Methane over Ni–Al₂O₃ and Ni–SiO₂ Catalysts: Role of Preparation Methods. *Catalysis Letters*, 150(8), 2180–2199. <https://doi.org/10.1007/S10562-020-03120-3/TABLES/6>
- Djinović, P., Batista, J., & Pintar, A. (2012). Efficient catalytic abatement of greenhouse gases: Methane reforming with CO₂ using a novel and thermally stable Rh–CeO₂ catalyst. *International Journal of Hydrogen Energy*, 37(3), 2699–2707. <https://doi.org/10.1016/J.IJHYDENE.2011.10.107>

- Gao, J., & 0000-0002-7726-4755. (2020). *A Study of Carbon Dioxide Catalytic Activation for its Conversion to Value-added Products*.
<https://harvest.usask.ca/handle/10388/13007>
- Gao, Y., Aihemaiti, A., Jiang, J., Meng, Y., Ju, T., Han, S., Chen, X., & Liu, J. (2020). Inspection over carbon deposition features of various nickel catalysts during simulated biogas dry reforming. *Journal of Cleaner Production*, 260, 120944.
<https://doi.org/10.1016/J.JCLEPRO.2020.120944>
- Gao, Y., Jiang, J., Meng, Y., Yan, F., & Aihemaiti, A. (2018). A review of recent developments in hydrogen production via biogas dry reforming. In *Energy Conversion and Management* (Vol. 171, pp. 133–155). Elsevier Ltd.
<https://doi.org/10.1016/j.enconman.2018.05.083>
- García-Diéguez, M., Herrera, C., Larrubia, M. Á., & Alemany, L. J. (2012). CO₂-reforming of natural gas components over a highly stable and selective NiMg/Al₂O₃ nanocatalyst. *Catalysis Today*, 197(1), 50–57.
<https://doi.org/10.1016/J.CATTOD.2012.06.019>
- Ghelamallah, M., & Granger, P. (2014). Supported-induced effect on the catalytic properties of Rh and Pt-Rh particles deposited on La₂O₃ and mixed α -Al₂O₃-La₂O₃ in the dry reforming of methane. *Applied Catalysis A: General*, 485, 172–180.
<https://doi.org/10.1016/J.APCATA.2014.07.021>
- Ghods, B., Meshkani, F., & Rezaei, M. (2016). Effects of alkaline earth promoters on the catalytic performance of the nickel catalysts supported on high surface area mesoporous magnesium silicate in dry reforming reaction. *International Journal of Hydrogen Energy*, 41(48), 22913–22921.
<https://doi.org/10.1016/J.IJHYDENE.2016.10.020>
- Guo, J., Lou, H., Zhao, H., Chai, D., & Zheng, X. (2004). Dry reforming of methane over nickel catalysts supported on magnesium aluminate spinels. *Applied Catalysis A: General*, 273(1–2), 75–82. <https://doi.org/10.1016/J.APCATA.2004.06.014>
- Huang, Q., Fang, X., Cheng, Q., Li, Q., Xu, X., Xu, L., Liu, W., Gao, Z., Zhou, W., &

- Wang, X. (2017). Synthesis of a Highly Active and Stable Nickel-Embedded Alumina Catalyst for Methane Dry Reforming: On the Confinement Effects of Alumina Shells for Nickel Nanoparticles. *ChemCatChem*, 9(18), 3563–3571. <https://doi.org/10.1002/CCTC.201700490>
- Jablonski, W. S., Villano, S. M., & Dean, A. M. (2015). A comparison of H₂S, SO₂, and COS poisoning on Ni/YSZ and Ni/K₂O-CaAl₂O₄ during methane steam and dry reforming. *Applied Catalysis A: General*, 502, 399–409. <https://doi.org/10.1016/J.APCATA.2015.06.009>
- Jang, W. J., Shim, J. O., Kim, H. M., Yoo, S. Y., & Roh, H. S. (2019). A review on dry reforming of methane in aspect of catalytic properties. *Catalysis Today*, 324, 15–26. <https://doi.org/10.1016/J.CATTOD.2018.07.032>
- Jawad, A., Rezaei, F., & Rownaghi, A. A. (2019). Highly efficient Pt/Mo-Fe/Ni-based Al₂O₃-CeO₂ catalysts for dry reforming of methane. <https://doi.org/10.1016/j.cattod.2019.06.004>
- Jawad, A., Rezaei, F., & Rownaghi, A. A. (2020). Highly efficient Pt/Mo-Fe/Ni-based Al₂O₃-CeO₂ catalysts for dry reforming of methane. *Catalysis Today*, 350, 80–90. <https://doi.org/10.1016/J.CATTOD.2019.06.004>
- Kamieniak, J., Bernalte, E., Doyle, A. M., Kelly, P. J., & Banks, C. E. (2017). Can Ultrasound or pH Influence Pd Distribution on the Surface of HAP to Improve Its Catalytic Properties in the Dry Reforming of Methane? *Catalysis Letters*, 147(8), 2200–2208. <https://doi.org/10.1007/S10562-017-2114-5/FIGURES/7>
- Kang, K. M., Kim, H. W., Shim, I. W., & Kwak, H. Y. (2011). Catalytic test of supported Ni catalysts with core/shell structure for dry reforming of methane. *Fuel Processing Technology*, 92(6), 1236–1243. <https://doi.org/10.1016/J.FUPROC.2011.02.007>
- Kaviani, M., Rezaei, M., Mehdi Alavi, S., & Akbari, E. (2022). High coke resistance Ni-SiO₂@SiO₂ core-shell catalyst for biogas dry reforming: Effects of Ni loading and calcination temperature. *Fuel*, 330, 125609. <https://doi.org/10.1016/J.FUEL.2022.125609>

- Khajenoori, M., Rezaei, M., & Meshkani, F. (n.d.). *Dry reforming over CeO₂-promoted Ni/MgO nano-catalyst: Effect of Ni loading and CH₄/CO₂ molar ratio*. <https://doi.org/10.1016/j.jiec.2014.03.043>
- Khavarian, M., Chai, S. P., & Mohamed, A. R. (2015). The effects of process parameters on carbon dioxide reforming of methane over Co–Mo–MgO/MWCNTs nanocomposite catalysts. *Fuel*, *158*, 129–138. <https://doi.org/10.1016/J.FUEL.2015.05.021>
- Li, L., Zhou, L., Ould-Chikh, S., Anjum, D. H., Kanoun, M. B., Scaranto, J., Hedhili, M. N., Khalid, S., Laveille, P. V., D'Souza, L., Clo, A., & Basset, J. M. (2015). Controlled Surface Segregation Leads to Efficient Coke-Resistant Nickel/Platinum Bimetallic Catalysts for the Dry Reforming of Methane. *ChemCatChem*, *7*(5), 819–829. <https://doi.org/10.1002/CCTC.201402965>
- Li, Y., Wang, Y., Zhang, X., & Mi, Z. (2008). Thermodynamic analysis of autothermal steam and CO₂ reforming of methane. *International Journal of Hydrogen Energy*, *33*(10), 2507–2514. <https://doi.org/10.1016/J.IJHYDENE.2008.02.051>
- Li, Z., Wang, Z., & Kawi, S. (2019). Sintering and Coke Resistant Core/Yolk Shell Catalyst for Hydrocarbon Reforming. *ChemCatChem*, *11*(1), 202–224. <https://doi.org/10.1002/CCTC.201801266>
- Macario, A., Frontera, P., Candamano, S., Crea, F., Luca, P. De, & Antonucci, P. L. (2019). Nanostructured Catalysts for Dry-Reforming of Methane. In *Journal of Nanoscience and Nanotechnology* (Vol. 19, Issue 6, pp. 3135–3147). American Scientific Publishers. <https://doi.org/10.1166/jnn.2019.16651>
- Mirzaei, F., Rezaei, M., & Meshkani, F. (2014). Coprecipitated Ni-Co Bimetallic Nanocatalysts for Methane Dry Reforming. *Chemical Engineering & Technology*, *37*(6), 973–978. <https://doi.org/10.1002/CEAT.201300729>
- Mirzaei, F., Rezaei, M., Meshkani, F., & Fattah, Z. (2015). Carbon dioxide reforming of methane for syngas production over Co–MgO mixed oxide nanocatalysts. *Journal of Industrial and Engineering Chemistry*, *21*, 662–667.

<https://doi.org/10.1016/J.JIEC.2014.03.034>

Nematollahi, B., Rezaei, M., & Khajenoori, M. (2011). *Combined dry reforming and partial oxidation of methane to synthesis gas on noble metal catalysts.*

<https://doi.org/10.1016/j.ijhydene.2010.12.007>

Oliveira, A. C., Carvalho, D. C., De Souza, H. S. A., Filho, J. M., Oliveira, A. C., Campos, A., Milet, É. R. C., De Sousa, F. F., & Padron-Hernandez, E. (2014). A study on the modification of mesoporous mixed oxides supports for dry reforming of methane by Pt or Ru. *Applied Catalysis A: General*, 473, 132–145.

<https://doi.org/10.1016/J.APCATA.2013.12.031>

Pakhare, D., Shaw, C., Haynes, D., Shekhawat, D., & Spivey, J. (2013). Effect of reaction temperature on activity of Pt- and Ru-substituted lanthanum zirconate pyrochlores (La₂Zr₂O₇) for dry (CO₂) reforming of methane (DRM). *Journal of CO₂ Utilization*, 1, 37–42. <https://doi.org/10.1016/J.JCOU.2013.04.001>

Pakhare, D., & Spivey, J. (2014). A review of dry (CO₂) reforming of methane over noble metal catalysts. *Chemical Society Reviews*, 43(22), 7813–7837.

<https://doi.org/10.1039/C3CS60395D>

Rahbar Shamskar, F., Rezaei, M., & Meshkani, F. (2017). The influence of Ni loading on the activity and coke formation of ultrasound-assisted co-precipitated Ni–Al₂O₃ nanocatalyst in dry reforming of methane. *International Journal of Hydrogen Energy*, 42(7), 4155–4164. <https://doi.org/10.1016/J.IJHYDENE.2016.11.067>

Ramezani, Y., Meshkani, F., & Rezaei, M. (2018). Preparation and evaluation of mesoporous nickel and manganese bimetallic nanocatalysts in methane dry reforming process for syngas production. *Journal of Chemical Sciences*, 130(1), 1–10. <https://doi.org/10.1007/S12039-017-1410-3/FIGURES/9>

Rezaei, M., & Alavi, S. M. (2019). Dry reforming over mesoporous nanocrystalline 5% Ni/M-MgAl₂O₄ (M: CeO₂, ZrO₂, La₂O₃) catalysts. *International Journal of Hydrogen Energy*, 44(31), 16516–16525.

<https://doi.org/10.1016/J.IJHYDENE.2019.04.213>

- Rezaei, M., Alavi, S. M., Sahebdehfar, S., Bai, P., Liu, X., & Yan, Z. F. (2008). CO₂ reforming of CH₄ over nanocrystalline zirconia-supported nickel catalysts. *Applied Catalysis B: Environmental*, 77(3–4), 346–354. <https://doi.org/10.1016/J.APCATB.2007.08.004>
- Rezaei, M., Alavi, S. M., Sahebdehfar, S., & Yan, Z. F. (2006). Nanocrystalline zirconia as support for nickel catalyst in methane reforming with CO₂. *Energy and Fuels*, 20(3), 923–929. <https://doi.org/10.1021/EF050384K/ASSET/IMAGES/LARGE/EF050384KF00010.JPEG>
- Rosha, P., Mohapatra, S. K., Mahla, S. K., & Dhir, A. (2019). Catalytic reforming of synthetic biogas for hydrogen enrichment over Ni supported on ZnOCeO₂ mixed catalyst. *Biomass and Bioenergy*, 125, 70–78. <https://doi.org/10.1016/J.BIOMBIOE.2019.04.013>
- Rosset, M., Féris, L. A., & Perez-Lopez, O. W. (2020). Biogas dry reforming over Ni-Al catalyst: Suppression of carbon deposition by catalyst preparation and activation. *International Journal of Hydrogen Energy*, 45(11), 6549–6562. <https://doi.org/10.1016/J.IJHYDENE.2019.12.207>
- Shakouri, M. 1985-. (2018). *Industrial Ni-Based Catalyst Development for Carbon Dioxide Reforming of Methane*. <https://harvest.usask.ca/handle/10388/8658>
- Shiraz, M. H. A., Rezaei, M., & Meshkani, F. (2016). The effect of promoters on the CO₂ reforming activity and coke formation of nanocrystalline Ni/Al₂O₃ catalysts prepared by microemulsion method. *Korean Journal of Chemical Engineering* 2016 33:12, 33(12), 3359–3366. <https://doi.org/10.1007/S11814-016-0203-6>
- Singha, R. K., Yadav, A., Shukla, A., Kumar, M., & Bal, R. (2017). Low temperature dry reforming of methane over Pd-CeO₂ nanocatalyst. *Catalysis Communications*, 92, 19–22. <https://doi.org/10.1016/J.CATCOM.2016.12.019>
- Tavanarad, M., Meshkani, F., & Rezaei, M. (2018). Synthesis and Application of Noble Metal Nanocatalysts Supported on MgAl₂O₄ in Glycerol Dry Reforming Reaction.

- Catalysis Letters*, 148(1), 164–172. <https://doi.org/10.1007/S10562-017-2221-3/FIGURES/9>
- Tian, Y., Ma, X., Chen, X., & Zhang, C. (2022). Effect of Ni-Co bimetallic core-shell catalyst for coke resistance in CO₂ reforming of biomass Tar. *Journal of Analytical and Applied Pyrolysis*, 164, 105539. <https://doi.org/10.1016/J.JAAP.2022.105539>
- Turap, Y., Wang, I., Fu, T., Wu, Y., Wang, Y., & Wang, W. (2020). Co–Ni alloy supported on CeO₂ as a bimetallic catalyst for dry reforming of methane. *International Journal of Hydrogen Energy*, 45(11), 6538–6548. <https://doi.org/10.1016/J.IJHYDENE.2019.12.223>
- Usman, M., Daud, W. M. A. W., & Abbas, H. F. (2015). *Dry reforming of methane: Influence of process parameters-A review*. <https://doi.org/10.1016/j.rser.2015.02.026>
- Wang, C., Jie, X., Qiu, Y., Zhao, Y., Al-Megren, H. A., Alshihri, S., Edwards, P. P., & Xiao, T. (2019). The importance of inner cavity space within Ni@SiO₂ nanocapsule catalysts for excellent coking resistance in the high-space-velocity dry reforming of methane. *Applied Catalysis B: Environmental*, 259, 118019. <https://doi.org/10.1016/J.APCATB.2019.118019>
- Wang, F., Xu, L., & Shi, W. (2016). Syngas production from CO₂ reforming with methane over core-shell Ni@SiO₂ catalysts. *Journal of CO₂ Utilization*, 16, 318–327. <https://doi.org/10.1016/J.JCOU.2016.09.001>
- Wang, H., Miller, J. T., Shakouri, M., Xi, C., Wu, T., Zhao, H., & Akatay, M. C. (2013). XANES and EXAFS studies on metal nanoparticle growth and bimetallic interaction of Ni-based catalysts for CO₂ reforming of CH₄. *Catalysis Today*, 207, 3–12. <https://doi.org/10.1016/J.CATTOD.2012.09.015>
- Yabe, T., & Sekine, Y. (2018). *Methane conversion using carbon dioxide as an oxidizing agent: A review*. <https://doi.org/10.1016/j.fuproc.2018.09.014>
- Yentekakis, I. V., Goula, G., Panagiotopoulou, P., Katsoni, A., Diamadopoulos, E., Mantzavinos, D., & Delimitis, A. (2015). Dry reforming of methane: Catalytic performance and stability of Ir catalysts supported on γ -Al₂O₃, Zr_{0.92}Y_{0.08}O_{2- δ}

- (YSZ) or Ce_{0.9}Gd_{0.1}O_{2-δ} (GDC) supports. *Topics in Catalysis*, 58(18–20), 1228–1241. <https://doi.org/10.1007/S11244-015-0490-X/TABLES/3>
- Yu, J., Feng, B., Liu, S., Mu, X., Lester, E., & Wu, T. (2022). Highly active Ni/Al₂O₃ catalyst for CO₂ methanation by the decomposition of Ni-MOF@Al₂O₃ precursor via cold plasma. *Applied Energy*, 315, 119036. <https://doi.org/10.1016/J.APENERGY.2022.119036>
- Zhan, Y., Han, J., Bao, Z., Cao, B., Li, Y., Street, J., & Yu, F. (2017). Biogas reforming of carbon dioxide to syngas production over Ni-Mg-Al catalysts. *Molecular Catalysis*, 436, 248–258. <https://doi.org/10.1016/J.MCAT.2017.04.032>
- Zhang, J., & Li, F. (2015). Coke-resistant Ni@SiO₂ catalyst for dry reforming of methane. *Applied Catalysis B: Environmental*, 176–177, 513–521. <https://doi.org/10.1016/J.APCATB.2015.04.039>
- Zhang, J., Wang, H., & Dalai, A. K. (2007). Development of stable bimetallic catalysts for carbon dioxide reforming of methane. *Journal of Catalysis*, 249(2), 300–310. <https://doi.org/10.1016/J.JCAT.2007.05.004>
- Zhang, J., Wang, H., & Dalai, A. K. (2008). Effects of metal content on activity and stability of Ni-Co bimetallic catalysts for CO₂ reforming of CH₄. *Applied Catalysis A: General*, 339(2), 121–129. <https://doi.org/10.1016/J.APCATA.2008.01.027>
- ZHANG, R., XIA, G., LI, M., WU, Y., NIE, H., & LI, D. (2015). Effect of support on the performance of Ni-based catalyst in methane dry reforming. *Journal of Fuel Chemistry and Technology*, 43(11), 1359–1365. [https://doi.org/10.1016/S1872-5813\(15\)30040-2](https://doi.org/10.1016/S1872-5813(15)30040-2)
- Zhang, T., Liu, Z., Zhu, Y. A., Liu, Z., Sui, Z., Zhu, K., & Zhou, X. (2020). Dry reforming of methane on Ni-Fe-MgO catalysts: Influence of Fe on carbon-resistant property and kinetics. *Applied Catalysis B: Environmental*, 264, 118497. <https://doi.org/10.1016/J.APCATB.2019.118497>

Appendix A. Permission to use

The data used in this thesis were published in Elsevier Chemical Engineering Journal and Carbon dioxide capture and conversion book. As an author of the papers and Elsevier copy right, I got the permission to use them in my thesis.

Furthermore, I have used figures from other papers and got permission from the Fuel and Applied Catalysis A journals.

Chemical Engineering Journal




Syngas production through dry reforming: A review on catalysts and their materials, preparation methods and reactor type
Author: Zahra Alipour, Venu Babu Borugadda, Hui Wang, Ajay K. Dalai
Publication: Chemical Engineering Journal
Publisher: Elsevier
Date: 15 January 2023
© 2022 Elsevier B.V. All rights reserved.

Journal Author Rights

Please note that, as the author of this Elsevier article, you retain the right to include it in a thesis or dissertation, provided it is not published commercially. Permission is not required, but please ensure that you reference the journal as the original source. For more information on this and on your other retained rights, please visit: <https://www.elsevier.com/about/our-business/policies/copyright#Author-rights>

[BACK](#) [CLOSE WINDOW](#)

Journal of Fuel



Effects of support modifiers on the catalytic performance of Ni/Al₂O₃ catalyst in CO₂ reforming of methane
Author: Zahra Alipour, Mehran Rezaei, Fereshteh Meshkani
Publication: Fuel
Publisher: Elsevier
Date: 1 August 2014
Copyright © 2014 Elsevier Ltd. All rights reserved.

Journal Author Rights

Please note that, as the author of this Elsevier article, you retain the right to include it in a thesis or dissertation, provided it is not published commercially. Permission is not required, but please ensure that you reference the journal as the original source. For more information on this and on your other retained rights, please visit: <https://www.elsevier.com/about/our-business/policies/copyright#Author-rights>

[BACK](#) [CLOSE WINDOW](#)

Elsevier: Carbon dioxide capture and conversion

11/23/22, 9:17 AM

Rightslink® by Copyright Clearance Center



[?](#) Help ▾ |
 [🗨️](#) Live Chat |
 [👤](#) Zahra Alipour ▾

Chapter:
Chapter 8 Dry reforming of methane and biogas to produce syngas: a review of catalysts and process conditions

Book: Carbon Dioxide Capture and Conversion

Author: Zahra Alipour, Venu Babu Borugadda, Hui Wang, Ajay K. Dalai

Publisher: Elsevier

Date: Jan 1, 2022

Copyright © 2022 Elsevier B.V. All rights reserved.

Order Completed

Thank you for your order.

This Agreement between Zahra Alipour ("You") and Elsevier ("Elsevier") consists of your order details and the terms and conditions provided by Elsevier and Copyright Clearance Center:

License number: Reference confirmation email for license number

License date: Nov, 23 2022

📖 Licensed Content

Licensed Content Publisher: Elsevier

Licensed Content Publication: Elsevier Books

Licensed Content Title: Carbon Dioxide Capture and Conversion

Licensed Content Author: Zahra Alipour, Venu Babu Borugadda, Hui Wang, Ajay K. Dalai

Licensed Content Date: 2022

Licensed Content Pages: 35

📋 Order Details

Type of Use: reuse in a thesis/dissertation

Portion: full chapter

Circulation: 1

Format: both print and electronic

Are you the author of this Elsevier chapter?: Yes

How many pages did you author in this Elsevier book?: 35

Will you be translating?: No

👤 About Your Work

Title: Performance of Ni alumina catalyst with core-shell and supported structures in dry reforming of methane

Institution name: University of Saskatchewan

Expected presentation date: Dec 2022

📁 Additional Data

<https://s100.copyright.com/AppDispatchServlet>

1/2

11/23/22, 9:17 AM

Rightslink® by Copyright Clearance Center

Requestor Location		Tax Details	
Requestor Location		Publisher Tax ID	GB 494 6272 12
Billing information		Price	
Billing Type	Invoice	Total	0.00 CAD
Billing address			
			Total: 0.00 CAD
CLOSE WINDOW			

© 2022 Copyright - All Rights Reserved | Copyright Clearance Center, Inc. | [Privacy statement](#) | [Data Security and Privacy](#)
| [For California Residents](#) | [Terms and Conditions](#) Comments? We would like to hear from you. E-mail us at customer-care@copyright.com

JOHN WILEY AND SONS LICENSE
TERMS AND CONDITIONS

Nov 30, 2022

This Agreement between Zahra Alipour ("You") and John Wiley and Sons ("John Wiley and Sons") consists of your license details and the terms and conditions provided by John Wiley and Sons and Copyright Clearance Center.

License Number 5438860438706

License date Nov 30, 2022

Licensed Content Publisher John Wiley and Sons

Licensed Content Publication ChemCatChem

Licensed Content Title Synthesis of a Highly Active and Stable Nickel-Embedded Alumina Catalyst for Methane Dry Reforming: On the Confinement Effects of Alumina Shells for Nickel Nanoparticles

Licensed Content Author Xiang Wang, Wufeng Zhou, Zhixian Gao, et al

Licensed Content Date Aug 7, 2017

Licensed Content Volume 9

Licensed Content 18

Issue

Licensed
Content 9
Pages

Type of use Dissertation/Thesis

Requestor
type University/Academic

Format Print and electronic

Portion Figure/table

Number of
figures/tables 1

Will you be
translating? No

Title Performance of Ni alumina catalyst with core-shell and supported structures in
dry reforming of methane

Institution
name University of Saskatchewan

Expected
presentation
date Dec 2022

Portions Figure 1

Requestor
Location

Publisher EU826007151
Tax ID

Total 0.00 CAD

Terms and Conditions

TERMS AND CONDITIONS

This copyrighted material is owned by or exclusively licensed to John Wiley & Sons, Inc. or one of its group companies (each a "Wiley Company") or handled on behalf of a society with which a Wiley Company has exclusive publishing rights in relation to a particular work (collectively "WILEY"). By clicking "accept" in connection with completing this licensing transaction, you agree that the following terms and conditions apply to this transaction (along with the billing and payment terms and conditions established by the Copyright Clearance Center Inc., ("CCC's Billing and Payment terms and conditions"), at the time that you opened your RightsLink account (these are available at any time at <http://myaccount.copyright.com>).

Terms and Conditions

- The materials you have requested permission to reproduce or reuse (the "Wiley Materials") are protected by copyright.
- You are hereby granted a personal, non-exclusive, non-sub licensable (on a stand-alone basis), non-transferable, worldwide, limited license to reproduce the Wiley Materials for the purpose specified in the licensing process. This license, **and any CONTENT (PDF or image file) purchased as part of your order**, is for a one-time use only and limited to any maximum distribution number specified in the license. The first instance of republication or reuse granted by this license must be completed within two years of the date of the grant of this license (although copies prepared before the end date may be distributed thereafter). The Wiley Materials shall not be used in any other manner or for any other purpose, beyond what is granted in the license. Permission is granted subject to an appropriate acknowledgement given to the author, title of the material/book/journal and the publisher. You shall also duplicate the copyright notice that appears in the Wiley publication in your use of the Wiley Material. Permission is also granted on the understanding that nowhere in the text is a previously published source acknowledged for all or part of this Wiley Material. Any third party content is expressly excluded from this permission.
- With respect to the Wiley Materials, all rights are reserved. Except as expressly granted by the terms of the license, no part of the Wiley Materials may be copied, modified, adapted (except for minor reformatting required by the new Publication), translated, reproduced, transferred or distributed, in any form or by any means, and no derivative works may be made based on the Wiley Materials without the prior permission of the respective copyright owner. **For STM Signatory Publishers clearing permission under the terms of the [STM Permissions Guidelines](#) only, the terms of the license are extended to include subsequent editions and for editions in other languages, provided such editions are for the work as a whole in situ and does not involve the separate exploitation of the permitted figures or extracts,**

You may not alter, remove or suppress in any manner any copyright, trademark or other notices displayed by the Wiley Materials. You may not license, rent, sell, loan, lease, pledge, offer as security, transfer or assign the Wiley Materials on a stand-alone basis, or any of the rights granted to you hereunder to any other person.

- The Wiley Materials and all of the intellectual property rights therein shall at all times remain the exclusive property of John Wiley & Sons Inc, the Wiley Companies, or their respective licensors, and your interest therein is only that of having possession of and the right to reproduce the Wiley Materials pursuant to Section 2 herein during the continuance of this Agreement. You agree that you own no right, title or interest in or to the Wiley Materials or any of the intellectual property rights therein. You shall have no rights hereunder other than the license as provided for above in Section 2. No right, license or interest to any trademark, trade name, service mark or other branding ("Marks") of WILEY or its licensors is granted hereunder, and you agree that you shall not assert any such right, license or interest with respect thereto
- NEITHER WILEY NOR ITS LICENSORS MAKES ANY WARRANTY OR REPRESENTATION OF ANY KIND TO YOU OR ANY THIRD PARTY, EXPRESS, IMPLIED OR STATUTORY, WITH RESPECT TO THE MATERIALS OR THE ACCURACY OF ANY INFORMATION CONTAINED IN THE MATERIALS, INCLUDING, WITHOUT LIMITATION, ANY IMPLIED WARRANTY OF MERCHANTABILITY, ACCURACY, SATISFACTORY QUALITY, FITNESS FOR A PARTICULAR PURPOSE, USABILITY, INTEGRATION OR NON-INFRINGEMENT AND ALL SUCH WARRANTIES ARE HEREBY EXCLUDED BY WILEY AND ITS LICENSORS AND WAIVED BY YOU.
- WILEY shall have the right to terminate this Agreement immediately upon breach of this Agreement by you.
- You shall indemnify, defend and hold harmless WILEY, its Licensors and their respective directors, officers, agents and employees, from and against any actual or threatened claims, demands, causes of action or proceedings arising from any breach of this Agreement by you.
- IN NO EVENT SHALL WILEY OR ITS LICENSORS BE LIABLE TO YOU OR ANY OTHER PARTY OR ANY OTHER PERSON OR ENTITY FOR ANY SPECIAL, CONSEQUENTIAL, INCIDENTAL, INDIRECT, EXEMPLARY OR PUNITIVE DAMAGES, HOWEVER CAUSED, ARISING OUT OF OR IN CONNECTION WITH THE DOWNLOADING, PROVISIONING, VIEWING OR USE OF THE MATERIALS REGARDLESS OF THE FORM OF ACTION, WHETHER FOR BREACH OF CONTRACT, BREACH OF WARRANTY, TORT, NEGLIGENCE, INFRINGEMENT OR OTHERWISE (INCLUDING, WITHOUT LIMITATION, DAMAGES BASED ON LOSS OF PROFITS, DATA, FILES, USE, BUSINESS OPPORTUNITY OR CLAIMS OF THIRD PARTIES), AND WHETHER OR NOT THE PARTY HAS BEEN ADVISED OF THE POSSIBILITY OF SUCH DAMAGES. THIS LIMITATION SHALL APPLY NOTWITHSTANDING ANY FAILURE OF ESSENTIAL PURPOSE OF ANY LIMITED REMEDY PROVIDED HEREIN.
- Should any provision of this Agreement be held by a court of competent jurisdiction to be illegal, invalid, or unenforceable, that provision shall be deemed amended to achieve as nearly as possible the same economic effect as the original provision, and the legality, validity and enforceability of the remaining provisions of this Agreement

shall not be affected or impaired thereby.

- The failure of either party to enforce any term or condition of this Agreement shall not constitute a waiver of either party's right to enforce each and every term and condition of this Agreement. No breach under this agreement shall be deemed waived or excused by either party unless such waiver or consent is in writing signed by the party granting such waiver or consent. The waiver by or consent of a party to a breach of any provision of this Agreement shall not operate or be construed as a waiver of or consent to any other or subsequent breach by such other party.
- This Agreement may not be assigned (including by operation of law or otherwise) by you without WILEY's prior written consent.
- Any fee required for this permission shall be non-refundable after thirty (30) days from receipt by the CCC.
- These terms and conditions together with CCC's Billing and Payment terms and conditions (which are incorporated herein) form the entire agreement between you and WILEY concerning this licensing transaction and (in the absence of fraud) supersedes all prior agreements and representations of the parties, oral or written. This Agreement may not be amended except in writing signed by both parties. This Agreement shall be binding upon and inure to the benefit of the parties' successors, legal representatives, and authorized assigns.
- In the event of any conflict between your obligations established by these terms and conditions and those established by CCC's Billing and Payment terms and conditions, these terms and conditions shall prevail.
- WILEY expressly reserves all rights not specifically granted in the combination of (i) the license details provided by you and accepted in the course of this licensing transaction, (ii) these terms and conditions and (iii) CCC's Billing and Payment terms and conditions.
- This Agreement will be void if the Type of Use, Format, Circulation, or Requestor Type was misrepresented during the licensing process.
- This Agreement shall be governed by and construed in accordance with the laws of the State of New York, USA, without regards to such state's conflict of law rules. Any legal action, suit or proceeding arising out of or relating to these Terms and Conditions or the breach thereof shall be instituted in a court of competent jurisdiction in New York County in the State of New York in the United States of America and each party hereby consents and submits to the personal jurisdiction of such court, waives any objection to venue in such court and consents to service of process by registered or certified mail, return receipt requested, at the last known address of such party.

WILEY OPEN ACCESS TERMS AND CONDITIONS

Wiley Publishes Open Access Articles in fully Open Access Journals and in Subscription journals offering Online Open. Although most of the fully Open Access journals publish open access articles under the terms of the Creative Commons Attribution (CC BY) License only, the subscription journals and a few of the Open Access Journals offer a choice of Creative Commons Licenses. The license type is clearly identified on the article.

The Creative Commons Attribution License

The [Creative Commons Attribution License \(CC-BY\)](#) allows users to copy, distribute and transmit an article, adapt the article and make commercial use of the article. The CC-BY license permits commercial and non-

Creative Commons Attribution Non-Commercial License

The [Creative Commons Attribution Non-Commercial \(CC-BY-NC\) License](#) permits use, distribution and reproduction in any medium, provided the original work is properly cited and is not used for commercial purposes.(see below)

Creative Commons Attribution-Non-Commercial-NoDerivs License

The [Creative Commons Attribution Non-Commercial-NoDerivs License \(CC-BY-NC-ND\)](#) permits use, distribution and reproduction in any medium, provided the original work is properly cited, is not used for commercial purposes and no modifications or adaptations are made. (see below)

Use by commercial "for-profit" organizations

Use of Wiley Open Access articles for commercial, promotional, or marketing purposes requires further explicit permission from Wiley and will be subject to a fee.

Further details can be found on Wiley Online Library
<http://olabout.wiley.com/WileyCDA/Section/id-410895.html>

Other Terms and Conditions:

v1.10 Last updated September 2015

Questions? customercare@copyright.com or +1-855-239-3415 (toll free in the US) or +1-978-646-2777.

Appendix B. MFC calibration

In order to calibrate mass flow controller (MFC), Mesalabs device (Figure B.1) was used to measure flow rate of different gases (N_2 , CH_4 , CO_2 , and H_2) at different channel. Ten different flow rate were set on MFC and actual flow rate were read on device. Figure B.2 shows different curve for each gases.



Figure B.1 Flow controller device

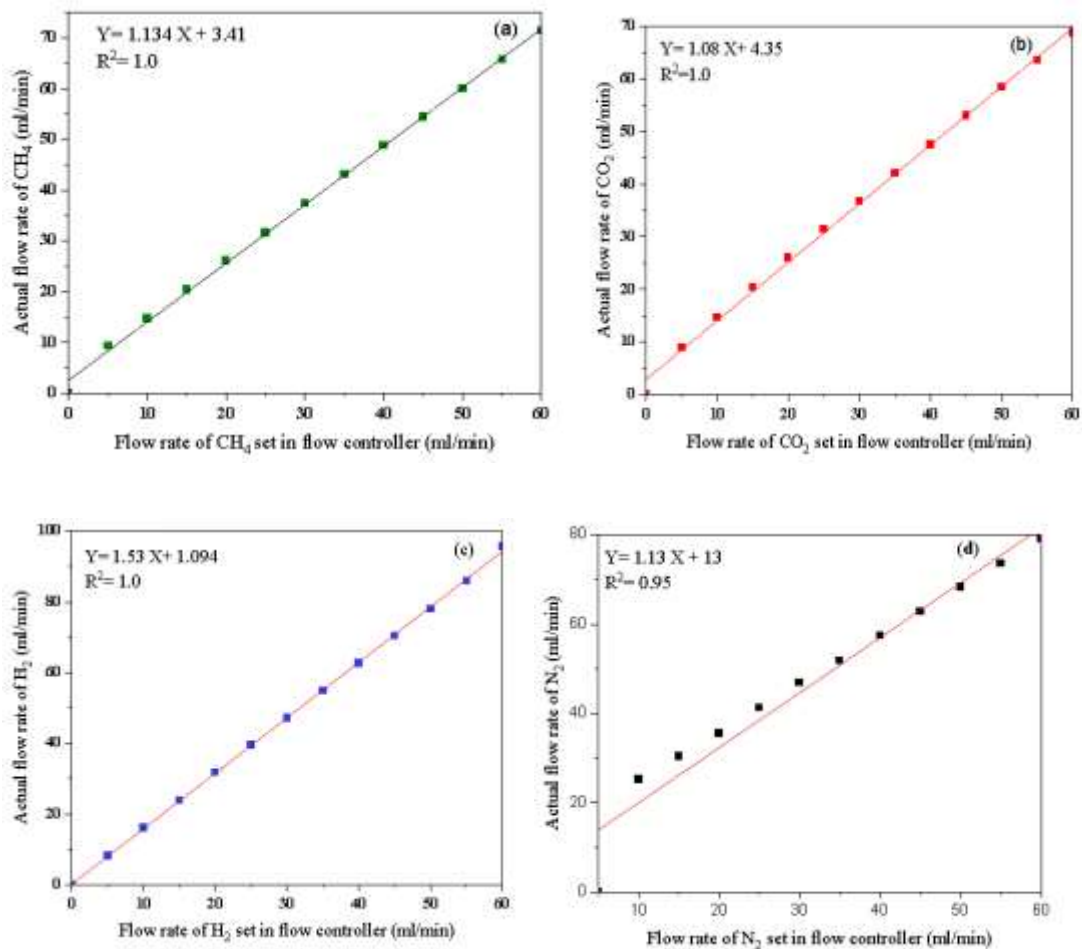
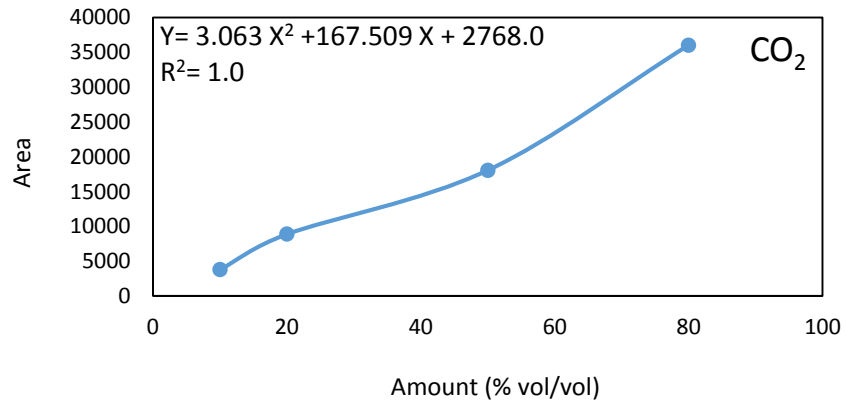
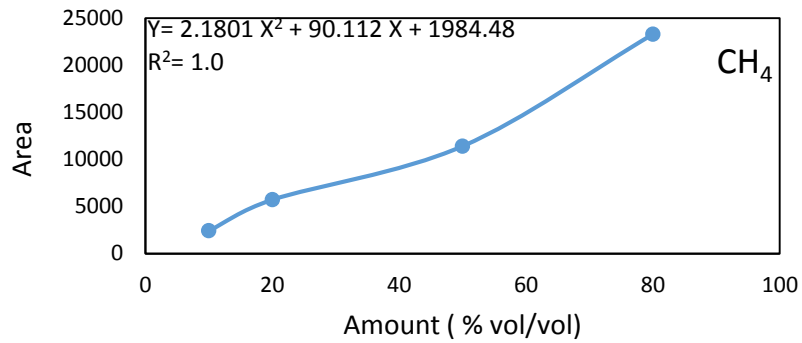


Figure B.2. MFC calibration curve

Appendix C. GC calibration

In order to calibrate GC, Gas with five different concentration was used with at least three injection at each concentration. The average area was calculated at each concentration to plot the Figure C.

1.



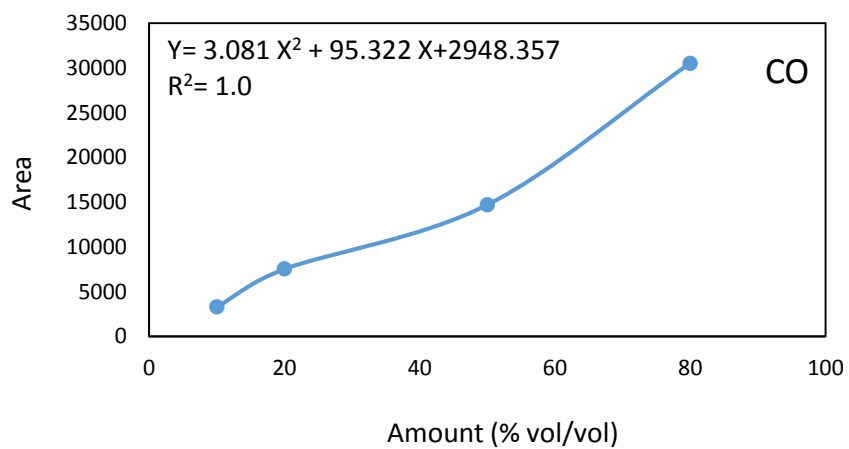
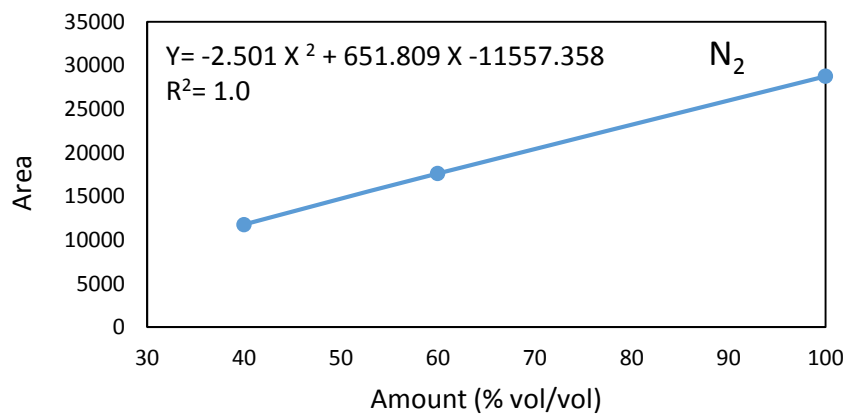
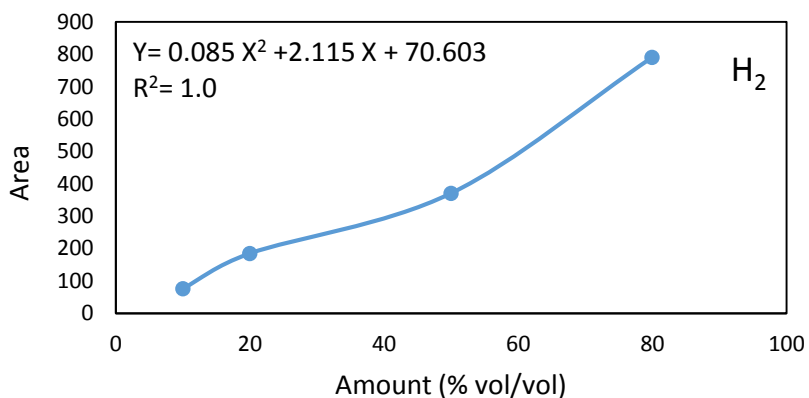


Figure C.1. GC calibration Curves

Appendix D. Temperature profile of the reactor

In order to obtain temperature profile of the reactor, different temperatures were set while N₂ gas was passing through the reactor. The inside temperature was measured in different position by K-type thermocouple. Figure a shows the relation between the set and actual temperatures and Figure D.1 illustrates temperature profile of the reactor.

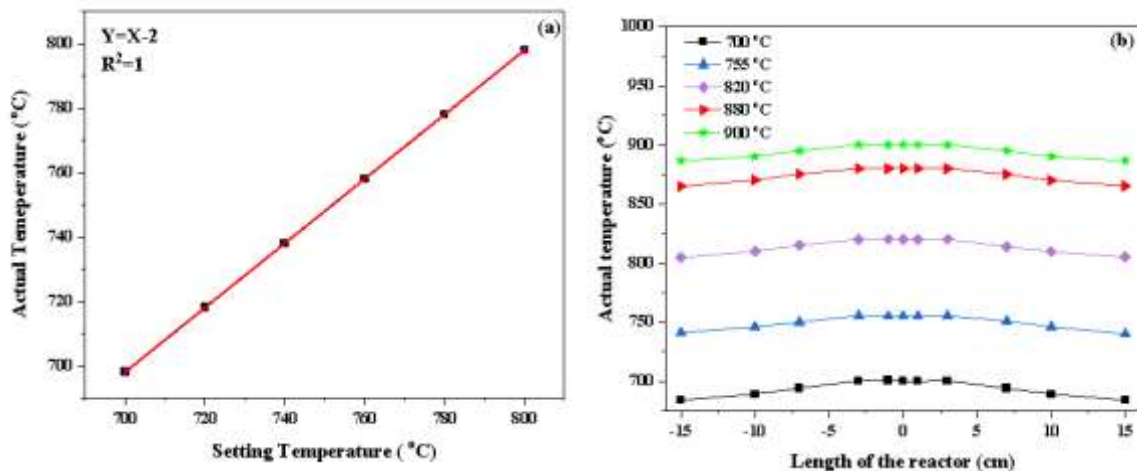


Figure D.1. (a) Furnace temperature calibration curve and (b) temperature profile of the reactor

Appendix E. Reproducibility of experimental results

H₂ Chemisorption: Hydrogen chemisorption was carried out twice to investigate the reproducibility of the results. Metal dispersion and their standard deviation (SD) (Equation E-1) results are listed in Table E. 1 for the core-shell catalysts. As it can be seen, SD for all samples is between 0 and 2, showing the results are near to mean.

$$SD = \sqrt{\frac{((X1-X)+(X2-X))^2}{2-1}} \quad (E-1)$$

Table E.1. Reproducibility results for Metal dispersion

Catalyst	Metal dispersion (%)		SD
	X1	X2	
5%Ni@Al ₂ O ₃	35.00	32.80	1.55
12%Ni@Al ₂ O ₃	12.20	13.06	0.60
20% @Ni@Al ₂ O ₃	5.10	5.12	0.01

Reproducibility results for CH₄ and CO₂ conversions are calculated and listed in Table E.2 for 12%Ni@Al₂O₃ catalyst during 24 h. As it is seen, SD for both conversion is between 0 and 1.

Table E.2. Reproducibility results for CH₄ and CO₂ conversions in 12%Ni@Al₂O₃ catalyst

	CH ₄ Conversion (%)		CO ₂ Conversion (%)	
	X1	X2	X1	X2
	38.6	39.2	41.6	42.4
SD	0.42		0.56	